

NUREG/CR-0213
(ORNL/NUREG/TM-202)

dy. 40



3 4456 0150240 8



Advanced Instrumentation for Reflood Studies Program Quarterly Progress Report, October 1-December 31, 1977

B. G. Eads

R. P. Gates

W. H. Leavell

J. E. Hardy

A. J. Moorhead

M. B. Herskovitz

C. S. Morgan

J. O. Hylton

M. J. Roberts

P. A. Jallouk

Prepared for the U.S. Nuclear Regulatory Commission
Office of Nuclear Regulatory Research
Under Interagency Agreements DOE 40-551-75 and 40-552-75

ORNL TECHNICAL INFORMATION
DIVISION

Y-12 TECHNICAL LIBRARY

Document Reference Section

LOAN COPY ONLY

Do NOT transfer this document to any other person. If you want others to see it, attach their names, return the document, and the Library will arrange the loan as requested.

UCN-1624
(3 5-60)

OAK RIDGE NATIONAL LABORATORY
OPERATED BY UNION CARBIDE CORPORATION · FOR THE DEPARTMENT OF ENERGY

Printed in the United States of America. Available from
National Technical Information Service
U.S. Department of Commerce
5285 Port Royal Road, Springfield, Virginia 22161

This report was prepared as an account of work sponsored by the United States Government. Neither the United States nor any of its employees, nor any of its contractors, subcontractors, or their employees, makes any warranty, express or implied, or assumes any legal liability or responsibility for the accuracy, completeness or usefulness of any information, apparatus, product or process disclosed, or represents that its use would not infringe privately owned rights.

NUREG/CR-0213
ORNL/NUREG/TM-202
Dist. Category R2

Contract No. W-7403-eng-26

INSTRUMENTATION AND CONTROLS DIVISION

ADVANCED INSTRUMENTATION FOR REFLOOD STUDIES PROGRAM
QUARTERLY PROGRESS REPORT, OCTOBER 1-DECEMBER 31, 1977

B. G. Eads, Manager

R. P. Gates	W. H. Leavell
J. E. Hardy	A. J. Moorhead
M. B. Herskovitz	C. S. Morgan
J. O. Hylton	M. J. Roberts
P. A. Jallouk	

Manuscript Completed - August 24, 1978

Date Published - September 1978

NOTICE: This document contains information of a preliminary nature. It is subject to revision or correction and therefore does not represent a final report.

Prepared for the
U.S. Nuclear Regulatory Commission
Office of Nuclear Regulatory Research
Under Interagency Agreements DOE 40-551-75 & 40-552-75
NRC FIN No. B0413

Prepared by the
OAK RIDGE NATIONAL LABORATORY
Oak Ridge, Tennessee 37830
operated by
UNION CARBIDE CORPORATION
for the
DEPARTMENT OF ENERGY



3 4456 0150240 8

•

•

•

•

•

•

CONTENTS

ABSTRACT.	1
KEYWORDS.	2
1. INTRODUCTION.	2
2. PROGRAM PLANNING AND ADMINISTRATION	4
3. HIGH-TEMPERATURE MATERIALS.	5
4. FILM PROBE DEVELOPMENT.	9
4.1 General Description of Probe	9
4.2 Mathematical Model of Probe.	10
4.3 Future Plans	18
5. STRING PROBE VELOCITY MEASUREMENT	19
5.1 Testing Procedure.	19
5.2 Results and Analysis — Steady-State Runs	23
5.3 Results and Analysis — Transient Runs.	34
6. STRING PROBE VOID FRACTION MEASUREMENT.	41
6.1 Testing Procedure.	41
6.2 Data Reduction and Analysis.	41
7. IN-BUNDLE PROBE VELOCITY MEASUREMENT.	44
7.1 Testing Procedure.	44
7.2 Data Reduction and Analysis.	50
8. AIR-WATER TESTING SUMMARY AND CONCLUSIONS	52
9. ELECTRONIC CIRCUIT DEVELOPMENT.	53
10. ADVANCED INSTRUMENTATION FOR REFLOOD STUDIES STEAM-WATER TEST STAND.	56
REFERENCES.	59

■

▶

■

■

■

■

ADVANCED INSTRUMENTATION FOR REFLOOD STUDIES PROGRAM
QUARTERLY PROGRESS REPORT, OCTOBER 1-DECEMBER 31, 1977

B. G. Eads, Manager

R. P. Gates	W. H. Leavell
J. E. Hardy	A. J. Moorhead
M. B. Herskovitz	C. S. Morgan
J. O. Hylton	M. J. Roberts
P. A. Jallouk	

ABSTRACT

Sensor development is under way, with several configurations being tested in air and water to establish design requirements for both the film and impedance probes.

The results of several tests during the development of high-temperature materials have shown varying degrees of possibilities. However, to date, a material has not been identified that will withstand the severe thermal transients of 300°C (572°F)/sec without cracking after a minimum of quenching tests.

The use of an adaptive cross-correlation algorithm in tracking both 1-min and 30-sec transients yielded noise analysis velocity estimates that lie in between the liquid and vapor velocities.

The use of a conductivity measurement to determine void fraction yielded reasonable agreement when compared with gamma densitometer measured values. This technique, however, is based on a knowledge of water conductivity, which is very dependent on temperature.

The development of electronic circuitry was begun to measure those electrical properties of the impedance and film probes which vary as a result of the two-phase flow in their vicinity. Electrical properties of some preliminary probe models were measured under various conditions to establish reasonable ranges of electrical parameters on which to base circuit designs. Three general measurement ideas were considered. After some evaluation, one specific technique was chosen as the most promising. The breadboarding and prototype fabrication are under way to implement this technique.

The design for various subsystems of the AIRS Steam-Water Test Stand is under way. This facility will be used to do proof-of-operability testing of the instrument systems in two-phase steam-water flow prior to delivery to PKL-II.

Keywords: Two-phase flow, air-water test, Advanced Instrumentation for Reflood Studies, adaptive cross-correlation algorithm, noise analysis, impedance probe, film probe, transient, string probe, void fraction, air-water facility, gamma densitometer, synchronously demodulated, in-phase, quadrature, driven shield, and conductivity.

1. INTRODUCTION

B. G. Eads

The goal of the Advanced Instrumentation for Reflood Studies (AIRS) Program is to develop and supply instrumentation systems for measurement of three-dimensional two-phase flow parameters in the upper plenum and core of two German and two Japanese pressurized-water reactor loss-of-coolant accident (PWR LOCA) nonnuclear reflood test facilities. When development is completed, instrumentation systems will be designed and fabricated by ORNL to meet the specific requirements of each test facility.

The AIRS program is an integral part of the national program on water reactor safety sponsored by the United States Nuclear Regulatory Commission (USNRC). AIRS is also a part of the joint 3-D program on reflood phenomena being conducted between JAERI of Japan, Kraftwerk Union of West Germany, and the USNRC. Within ORNL there is an interface with the Advanced Two-Phase Flow Instrumentation Program and the Blowdown Heat Transfer (BDHT) Program in the sharing of an air-water test facility; a primary interface exists with the Film Probe Development Program at Lehigh University. In development of the film probe, ORNL will initially concentrate on high-temperature materials development, with Lehigh University doing further development of the basic concept.

Several different types of sensors and configurations are under development; however, all impedance sensors under development operate on the same principle. The sensor measures the electrical impedance between electrodes and, when suitably calibrated, the local void fraction. By cross-correlation of the electrical output of two sensors, the velocity and direction of the fluid can be inferred.

One type of sensor under development has electrodes in the form of bands around the circumference of a tube, that is, an instrumented guide tube. The electrode bands are flush with the surface of the tube and will provide interference-free installation into the core of a reflood facility. Other sensor designs call for electrodes in the form of prongs or flags which protrude from the tube surface. In concept, these electrodes would be mechanically attached to the tubes after installation in the grid spacers of the core assembly. The details of how this final assembly will be accomplished are yet to be determined. The guide tube probes will contain sensors and metal-sheathed thermocouples for local temperature readings near the sensors. The thermocouples and the metal-sheathed sensor leads are routed inside the tube and exit at the top or bottom of the guide tube.

Instrument systems for measuring two-phase flow velocities by correlation of signals from paired electrical conductivity probes have been considered by several investigators. One such system, called a string probe, produces highly coherent signals and was first considered by Carrard and Ledwidge.¹ Testing of a similar device was initiated in the Advanced Two-Phase Flow Instrumentation Program²⁻⁴ and is continuing under the AIRS program.

2. PROGRAM PLANNING AND ADMINISTRATION

B. G. Eads
R. P. Gates

The AIRS program was initiated in the last quarter of FY 1977. An assessment was completed of the state of the art of the technology of the impedance probe and film probe development as applicable to reflood studies. A scoping estimate of resource requirements to complete the work on the requested schedule was also completed. Existing calibration facilities in North America were surveyed, a preconceptual design and a cost estimate for a calibration facility were completed, and the ongoing development of impedance probes at ORNL was accelerated. Communications were established with the film probe development program at Lehigh University, and ORNL participation in this effort was defined. During the first quarter of FY 1978, development was further accelerated and the full staffing level was reached.

A critical path schedule was prepared which indicates the milestones and time frames necessary to achieve the critical shipping dates.

A steam-water test stand was targeted for completion in May 1978.

3. HIGH-TEMPERATURE MATERIALS

A. J. Moorhead*
C. S. Morgan*

The electrical insulation used in the film and impedance probes must be able to withstand exposure to hot steam [950°C (1742°F)] and severe thermal transients [300°C (572°F)/sec] in the PKL facility. Commonly used ceramic materials such as aluminum oxide and beryllium oxide will survive the hot steam but cannot withstand the thermal shock. Materials such as quartz, diamond, and boron nitride may survive the shock but are subject to some dissolving or leaching in hot water.

Several ceramic systems have been found which are impervious to thermal shock and appear able to survive in the hot steam; however, very little data on their physical and electrical properties in the presence of hot steam have been found in the literature. Therefore, a testing program is under way to determine which materials will be suitable for use in the PKL environment.

The thermal shock requirement means that the ceramic must have a very low (i.e., near zero) coefficient of thermal expansion or sufficient strength to withstand the thermal-gradient-induced stress. The adequacy of thermal shock resistance of candidate ceramics was tested by quenching from high temperature in water. Although higher temperatures were used initially, it was concluded that quenching from 500°C (932°F) into hot water would provide a sufficiently rigorous test. The approximate rate of cooling, determined by attaching a thermocouple to the specimen and recording the temperature with a digital transient recorder, was around

*Metals and Ceramics Division.

600°C (1112°F)/sec. The effect of thermal shock was evaluated on the basis of the appearance of microscopically visible cracks. Dye penetrant tests were not used since many of the ceramics tested were porous.

Materials evaluated include alumina and beryllia pieces for comparison. The tests include pieces from three ceramic systems that have very low thermal expansion: Cordierite, Al_2O_3 , MgO , SiO_2 (Alsimag 447 and 701), from Technical Ceramic Products Division of 3M; Rosolite, Al_2O_3 , SiO_2 , Li_2O , from Atomergic Chemetals Co., a division of Gallard-Schlesinger Chemical Mfg. Co.; and Ta_2WO_8 and $\text{Hf-Ta}_2\text{WO}_8$ specimens prepared by C. E. Holcomb at the Oak Ridge Y-12 Plant. A special type of cermet prepared by hot-pressing Al_2O_3 powder with small metal globules on the particle surfaces was tested. The globules were deposited in situ. Samples of these and other ceramics were subjected to a series of ten quenches; the results and conditions are described in Table 1.

Several of the specimens (hot-pressed Ta_2WO_8 , $\text{Hf-Ta}_2\text{WO}_8$, Cordierite, Rosolite, Al_2O_3 -Fe and Al_2O_3 -Pt cermets, and quartz) had no cracks, while the Si_3N_4 had only small cracks at the periphery. The quartz may not be usable since it is soluble in high-temperature water and the Al_2O_3 -Fe slowly oxidizes. Other specimens are being tested in a stream of high-temperature, superheated steam; preliminary results indicate very slow etching. These steam tests will be extended, and behavior in hot water will be evaluated. Some materials that are unaffected by steam may be vulnerable to hot water leaching.

The evaluation results so far indicate that many of the materials in Table 1 would be satisfactory. The only problem is that the materials that survived the thermal shock tests are slightly porous and will absorb

Table 1. Materials tested for thermal shock

Material	Coefficient of thermal expansion ($\Delta l/l \times 10^{-6}/K$)	Density (% of theoretical)	Results of thermal shock tests ^a
Aluminum oxide ^b	6.5	99+	Microscopic cracks visible after 1 quench
Beryllium oxide	8	99+	Microscopic cracks visible after 1 quench
Beryllium oxide	8	80+	Cracks visible after 2 or 3 quenches
Cordierite (Alsimag 701) 2MgO, 2Al ₂ O ₃ , 5SiO ₂	3.3	99	Cracks visible after 2 or 3 quenches
Cordierite (Alsimag 447)	1.5	85+	No cracks after 30 quenches
Rosolite (Al ₂ O ₃ , 4SiO ₂ , 9Li ₂ O)	<1	80	No cracks after 30 quenches
Rosolite	<1	99	Microscopic cracks visible after 2 quenches
Al ₂ O ₃ - 5% Fe	7	85	No cracks after 10 quenches
Al ₂ O ₃ - 1% Pt	6.5	85	No cracks after 10 quenches
Al ₂ O ₃ - 1% Pt	6.5	99	Cracks appeared after 3 quenches
Ta ₂ WO ₈	-2.1	90+	No cracks after 10 quenches
Hf-Ta ₂ WO ₈	0	60	No cracks after 10 quenches
Si ₃ N ₄	2.8	90+	Small cracks near edge after 10th quench
Quartz	19	100	No cracks after 10 quenches
MACOR (Corning glass ceramic)	9.4	100	Broke into pieces after second quench

^a Quenching from 500°C (932°F) into hot water.

^b Several types of Al₂O₃ were tested (including sapphire); all cracked.

a certain amount of water, thus changing the electrical properties.

Preliminary measurements have indicated that the effect of these changes on the overall instrument performance can be held to a tolerable level by using appropriate electrical measurement circuits.

4. FILM PROBE DEVELOPMENT

J. O. Hylton

4.1 General Description of Probe

The film probe is designed to measure the thickness and velocity of the condensate film that forms on various internal surfaces of the test vessel during the reflood portion of a PWR LOCA experiment. A typical probe configuration consists of two or more electrodes assembled in a ceramic insulator and mounted in the surface of interest so that the electrodes are flush with the surface. The electrical admittance (or impedance) between the electrodes varies with the thickness of the film over a range that depends on the electrode geometry. With appropriate calibration, a measurement of probe admittance will yield film thickness.

Probe calibrations are strongly dependent on the electrical properties (conductivity and permittivity) of the liquid film, the vapor phase above the film, and the ceramic insulating material. If these all remain constant, measurement of film thickness is a straightforward procedure. In concept, the film velocity may be measured by installing a second film probe at a known distance downstream from the first and introducing a known disturbance of short duration into the film upstream of the two probes. Velocity is obtained by cross-correlation of the two signals. The concepts being considered for introducing the disturbance are injection of a minute amount of electrolyte (salt solution) or by generating hydrogen bubbles in the film by electrolysis.

Basic development of the film probe is being done at Lehigh University. They are currently conducting an experimental program to

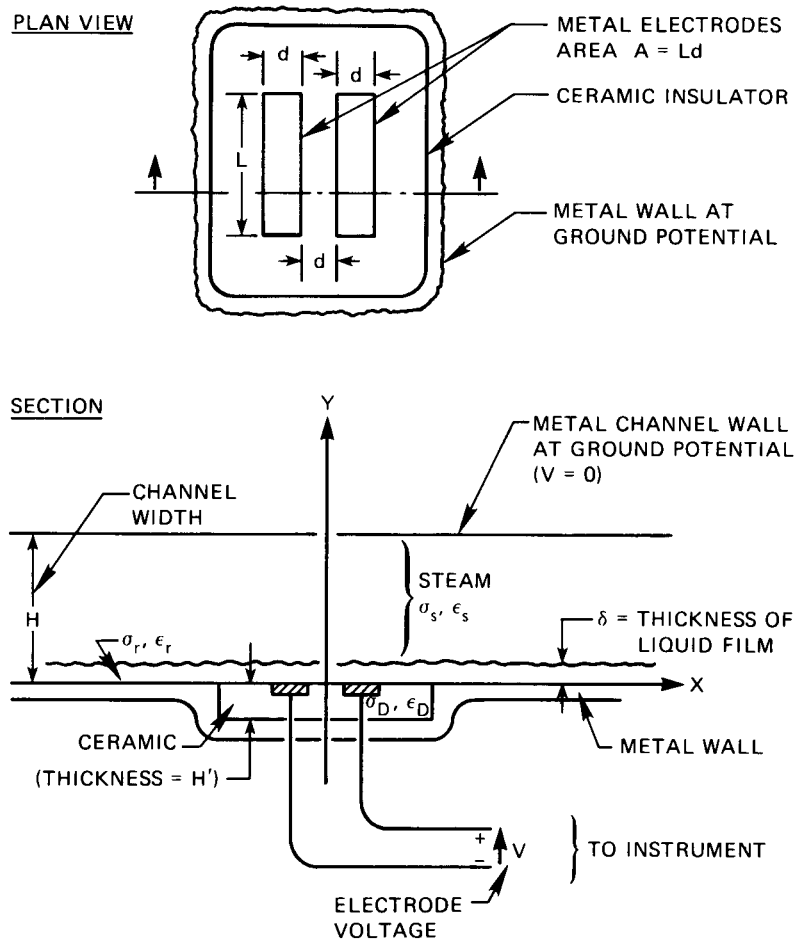
determine a suitable probe configuration for film thickness and velocity measurements in the German and Japanese reflood experiments. The probe concepts discussed above have worked successfully in air-water experiments at low temperatures [$<100^{\circ}\text{C}$ (212°F)]. However, several problems must be solved to make good measurements in high-temperature steam and water. Materials and fabrication problems were discussed earlier; some of the measurement problems and possible solutions will be discussed in this section.

4.2 Mathematical Model of Probe

To illustrate some of the potential measurement problems at high temperatures, a mathematical model was developed which approximates probe admittance as a function of film thickness. Figure 1 shows the electrode configuration for which the model was developed. The electrode-to-electrode impedance can be represented by an equivalent circuit consisting of a resistor R in parallel with a capacitor C . The admittance of the equivalent circuit is $Y = (1/R) + j\omega C$. The conductance ($1/R = G$) or the capacitance C is given by the following expressions:

$$G_n = \left\{ G/A/d = \sigma_D \sum_{n=1}^{\infty} b_n + \sigma_s \sum_{n=1}^{\infty} b_n e^{-(n\pi\delta/2d)} + \sigma_r \sum_{n=1}^{\infty} b_n \left[1 - e^{-(n\pi\delta/2d)} \right] \right\}, \quad (4.1)$$

$$C_n = \left\{ C/\epsilon_0 A/d = \epsilon_D \sum_{n=1}^{\infty} b_n + \epsilon_s \sum_{n=1}^{\infty} b_n e^{-(n\pi\delta/2d)} + \epsilon_r \sum_{n=1}^{\infty} b_n \left[1 - e^{-(n\pi\delta/2d)} \right] \right\}. \quad (4.2)$$



σ_r, ϵ_r — CONDUCTIVITY AND RELATIVE PERMITTIVITY OF LIQUID FILM (WATER)
 σ_D, ϵ_D — CONDUCTIVITY AND RELATIVE PERMITTIVITY OF CERAMIC INSULATOR
 σ_s, ϵ_s — CONDUCTIVITY AND RELATIVE PERMITTIVITY OF STEAM IN THE OPEN CHANNEL. IN SOME CASES A TWO-PHASE MIXTURE MAY EXIST IN THE CHANNEL. THESE SYMBOLS THEN REPRESENT AVERAGE PROPERTIES OF THE MIXTURE

Fig. 1. Typical film probe configuration.

All the symbols are explained in Fig. 1, with the exception of the coefficients b_n , which are determined by the electrode geometry.

The most obvious difficulty with these relations is their strong dependence on the electrical properties (σ, ϵ) of the materials involved. Both the relative conductivity and the relative permittivity of water

(σ_r, ϵ_r) and of the ceramic insulator (σ_D, ϵ_D) are known to vary rapidly with temperature. Figure 2 illustrates this variation for pure water and alumina.

Figures 3 and 4 illustrate the effect of temperature when the models of Eqs. (4.1) and (4.2) are used to calculate the probe capacitance and conductance.

The Lehigh researchers have developed a measurement circuit with an output signal proportional to the ratio of the admittances of two probes of different electrode spacing. The motivation for using a ratio circuit is that the effect of varying water properties $(\sigma_r$ and $\epsilon_r)$ will be greatly reduced while a fairly sensitive response to film thickness is retained.

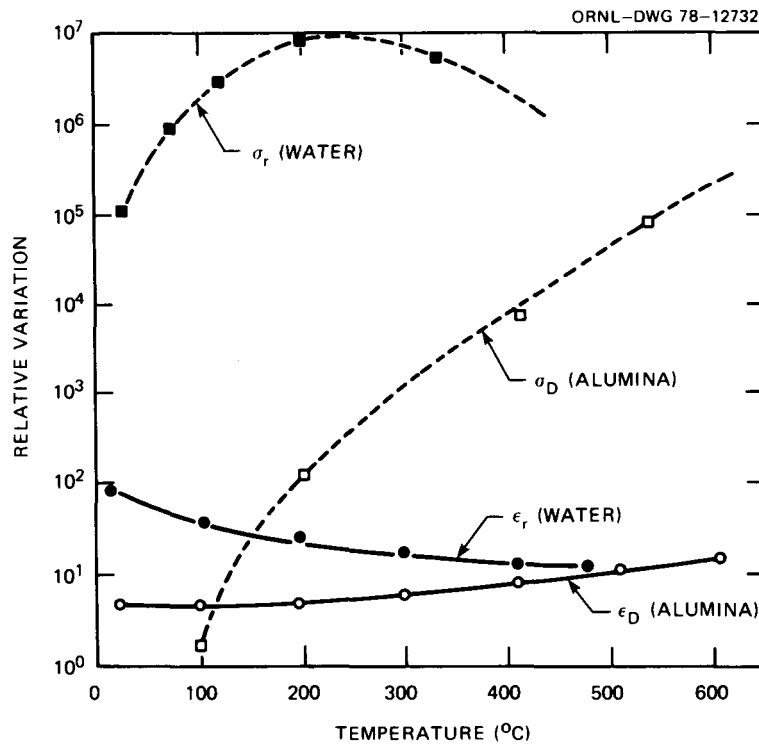


Fig. 2. Temperature dependence of electrical properties of water and a typical ceramic insulator.

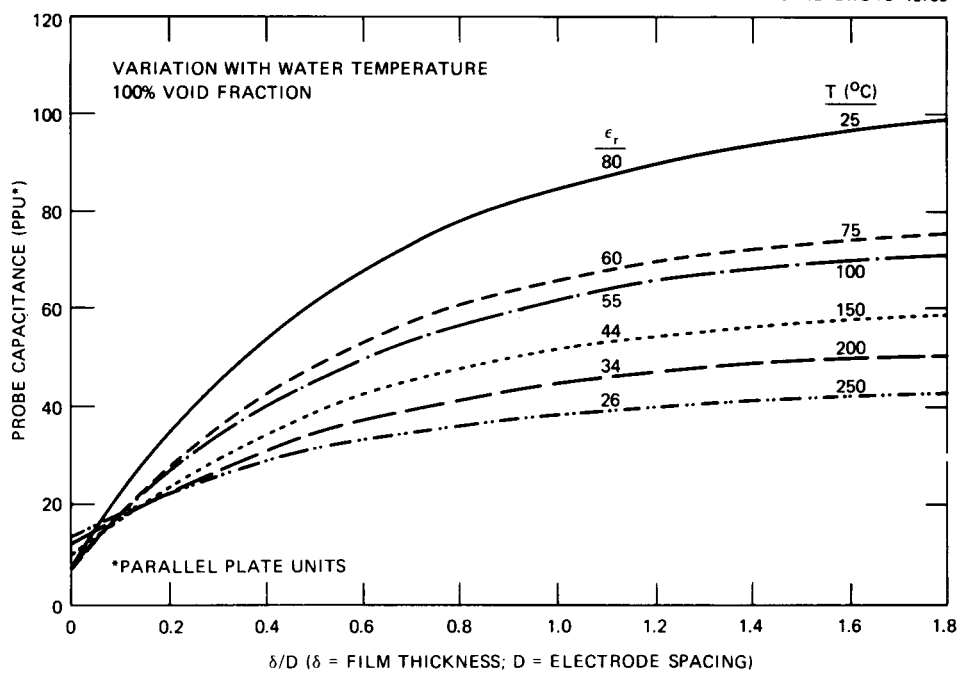


Fig. 3. Capacitance vs film thickness.

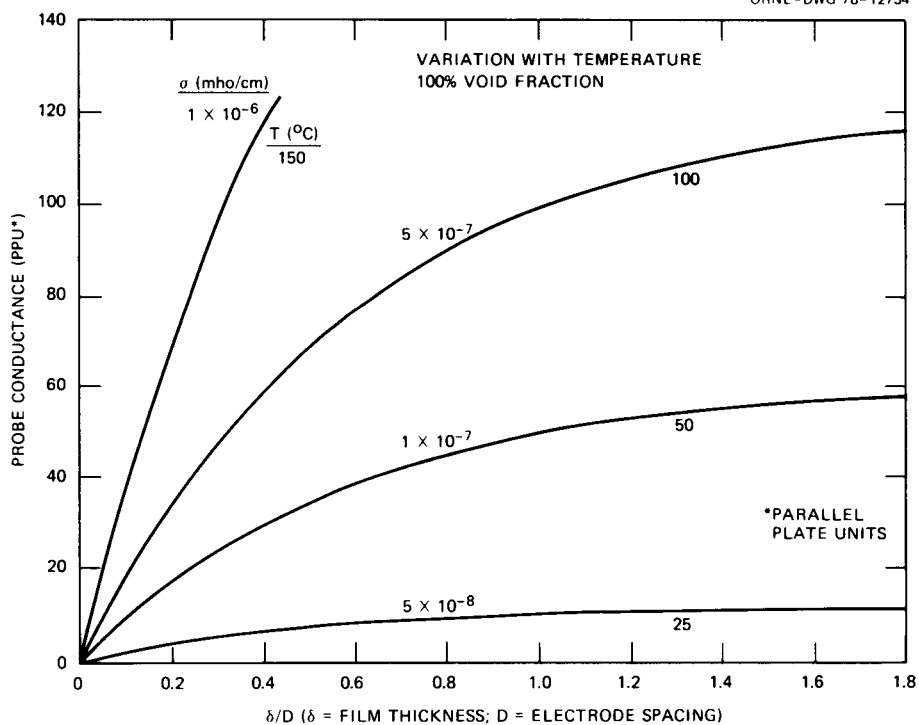


Fig. 4. Conductance vs film thickness.

Figure 5 shows that the calculated conductance ratio is essentially independent of temperature. Experimental data taken thus far at Lehigh tend to verify the functional behavior of these calculations.

The curves in Figs. 3 to 5 show only the effects of variations in the electrical properties of the liquid and the ceramic insulator. There is also a dependence on the properties (ϵ_s, σ_s) of the steam above the film. If this region contains pure steam, there will be very little variation with temperature. For all practical purposes, ϵ_s will remain 1 and σ_s will remain zero (compared to σ_r); however, there is a possibility that the region will contain a two-phase mixture of steam and water. Experience with the use of impedance probes indicates that significant changes in the average impedance of the mixture occur even for dispersed mist flow at high void fractions.

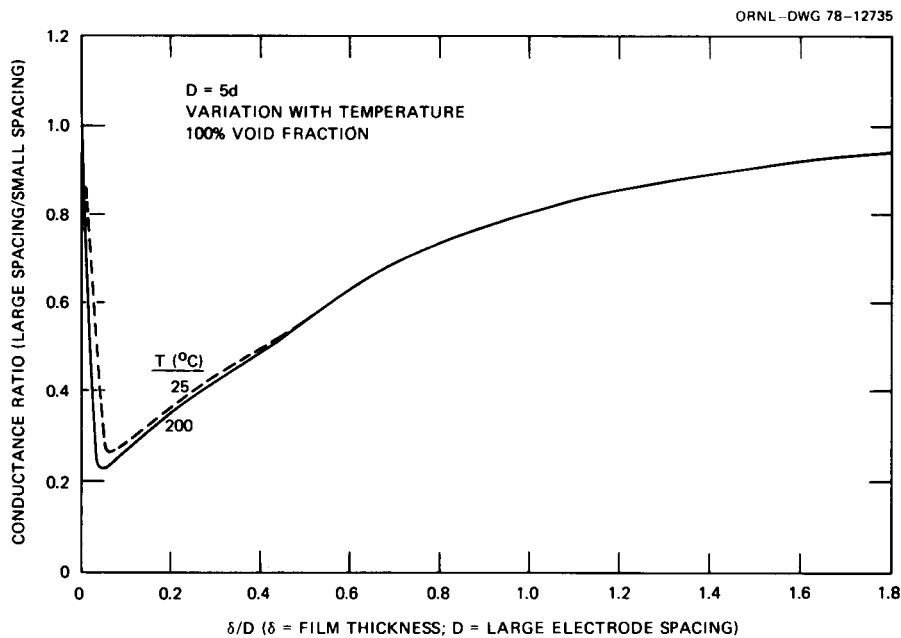


Fig. 5. Conductance ratio vs film thickness variation with temperature.

The functional relation between void fraction and the effective conductivity (σ_m) or the effective dielectric constant (ϵ_m) of the mixture is strongly dependent on the flow regime (i.e., dispersed flow or separated flow). For dispersed mist flow, the following equations derived by Maxwell relate the effective conductivity (σ_m) and dielectric constant (ϵ_m) of the mixture to void fraction:

$$\frac{\sigma_m - \sigma_s}{\sigma_m + 2\sigma_s} = (1 - \alpha) \frac{\sigma_r - \sigma_s}{\sigma_r + 2\sigma_s} \quad (4.3)$$

$$\frac{\epsilon_m - \epsilon_s}{\epsilon_m + 2\epsilon_s} = (1 - \alpha) \frac{\epsilon_r - \epsilon_s}{\epsilon_r + 2\epsilon_s} , \quad (4.4)$$

where

α = void fraction,

$\sigma_r = \sigma_{\text{water}}$,

$\sigma_s = \sigma_{\text{steam}}$,

$\epsilon_r = \epsilon_{\text{water}}$,

$\epsilon_s = \epsilon_{\text{steam}}$.

For conditions under which $\sigma_{\text{water}} \gg \sigma_{\text{steam}}$ and $\epsilon_{\text{water}} \gg \epsilon_{\text{steam}}$, these equations can be approximated by

$$\frac{\sigma_m}{\sigma_s} \approx \frac{3 - 2\alpha}{\alpha} \quad (4.5)$$

$$\frac{\epsilon_m}{\epsilon_s} \approx \frac{3 - 2\alpha}{\alpha} . \quad (4.6)$$

If these relations are incorporated into Eqs. (4.1) and (4.2), the dependence upon the void fraction of the two-phase mixture above the film

as well as film thickness can be seen:

$$G_n = \sigma_D \sum_{n=1}^{\infty} b_n + \sigma_s \left(\frac{3 - 2\alpha}{\alpha} \right) \sum_{n=1}^{\infty} b_n e^{-(n\pi\delta/2d)} + \sigma_r \sum_{n=1}^{\infty} b_n \left[1 - e^{-(n\pi\delta/2d)} \right], \quad (4.7)$$

$$C_n = \epsilon_D \sum_{n=1}^{\infty} b_n + \epsilon_s \frac{3 - 2\alpha}{\alpha} \sum_{n=1}^{\infty} b_n e^{-(n\pi\delta/2d)} + \epsilon_r \sum_{n=1}^{\infty} b_n \left[1 - e^{-(n\pi\delta/2d)} \right]. \quad (4.8)$$

Figures 6 and 7 show the effect of void fraction on the probe response as calculated using these equations.

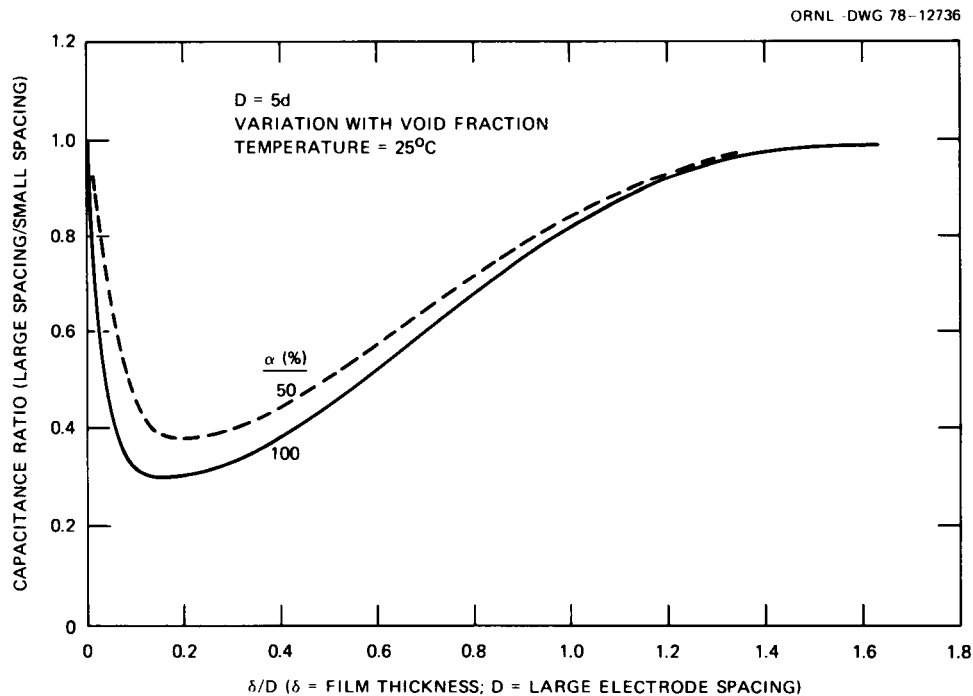


Fig. 6. Capacitance ratio vs film thickness (large spacing/small spacing).

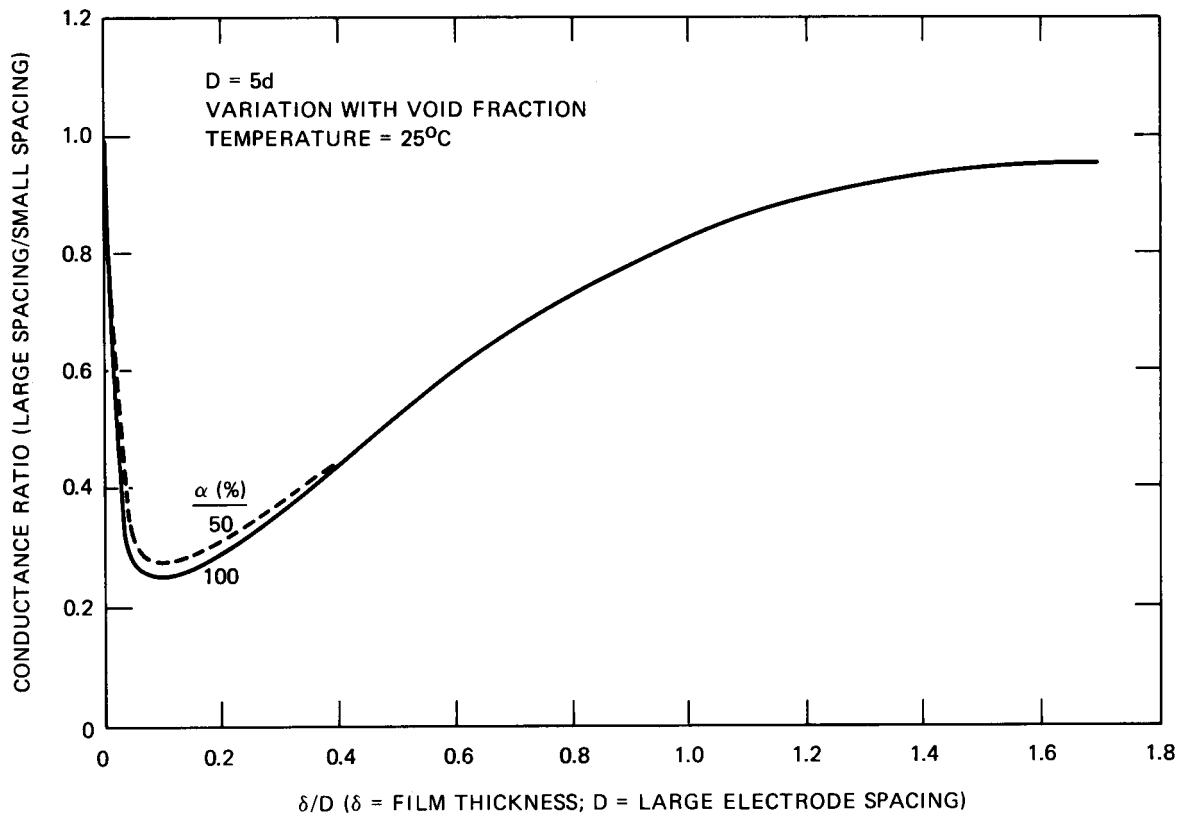


Fig. 7. Conductance ratio vs film thickness variation with void fraction.

In summary, mathematical models and experimental data taken at Lehigh University indicate that the dependence of the film probe response on the electrical properties of water can be greatly reduced by the conductance ratio technique. Preliminary calculations also show that the two-phase mixture above the film may introduce significant errors for capacitance measurements (Fig. 6) but not for conductance measurements (Fig. 7). The void fraction effect has not yet been experimentally verified; however, if it proves to be a significant source of error, an extra impedance probe may have to be placed in the channel above the film to measure the void fraction.

4.3 Future Plans

Researchers at Lehigh University plan to construct an apparatus that will permit probe calibrations at higher temperatures [100 to 170°C (212 to 338°F)]. They will continue work in this area as well as finalizing the velocity measurement technique for the PKL experiment. ORNL research is presently concentrated on the materials and fabrication problems for the high-temperature probes, and several low-temperature probes [200°C (392°F)] have been fabricated and sent to Lehigh for calibration.

5. STRING PROBE VELOCITY MEASUREMENT

J. E. Hardy* P. A. Jallouk* W. H. Leavell

5.1 Testing Procedure

The string probe (Fig. 8) consists of a set of 12 parallel 0.56-mm-diameter (0.022-in.) electrodes. These Nichrome wires detect fluctuations in electrical impedance in the flowing two-phase mixture. The parallel wires, installed in a 101-mm-ID (4-in.) section of clear plastic (Lucite)

* Engineering Technology Division.

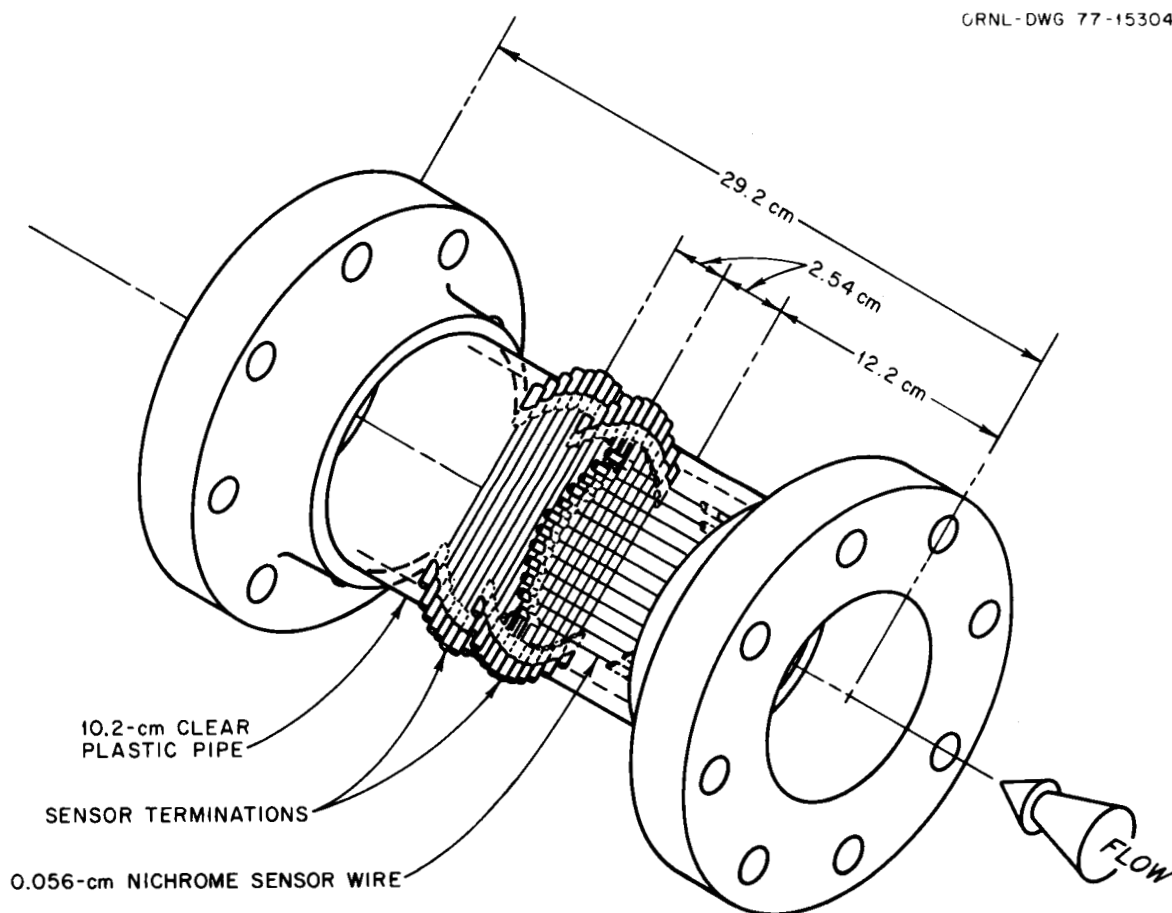


Fig. 8. String probes mounted in a Lucite spool piece.

pipe (Fig. 8), were spaced 7.6 mm (0.3 in.) apart in a plane perpendicular to the pipe axis. Figure 9 shows the wires electrically connected in a parallel plate fashion so that the impedance between any two wires in the flow can be monitored.

Preliminary results from the testing of the string probe were previously reported.⁴ Some discrepancies were noted between the predicted two-phase velocities and the velocity determined from noise-analysis techniques. This difference was at least partially attributed to the

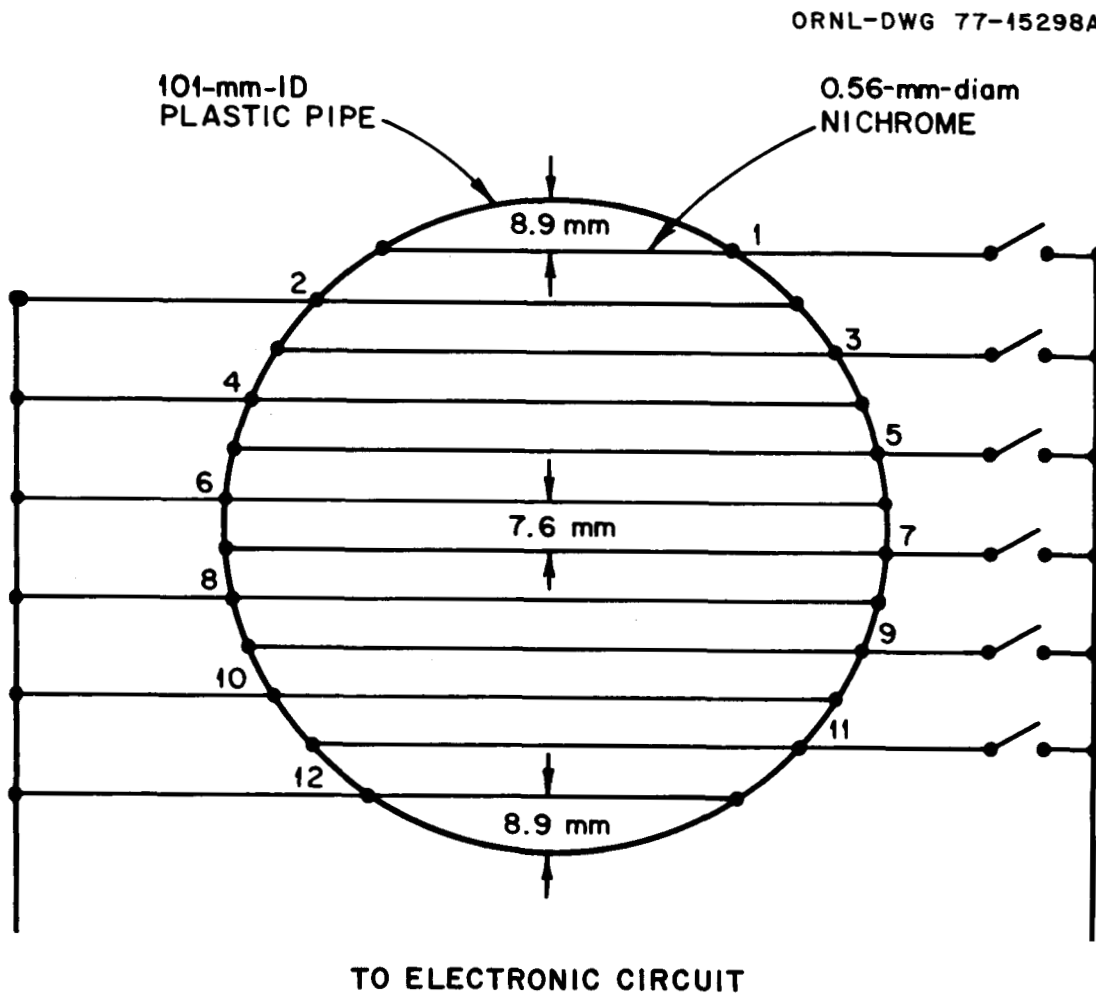


Fig. 9. Electrical connections of string probe wires.

proximity of the string probe to a bend in the piping system. As a result, the string probe was relocated away from the bend, and an instrumented spool piece containing a drag disk, a turbine meter, and a three-beam gamma densitometer was included in the system. Test loop instrumentation is shown in Table 2. Information from these instruments will supplement the flow measurements and could yield liquid and vapor velocity values. The string probe and the 16-rod bundle to be described later were tested in vertical upflow in air-water as shown in Fig. 10.

Table 2. Test loop instrumentation

Loop parameter	Instrumentation ^a
Water flow rate	0.000126 m ³ /sec (2 gpm) to 0.00631 m ³ /sec (100 gpm) Brooks rotameter
Air flow rate	Greater than 0.00755 m ³ /sec (16 scfm) critical flow orifices
Density	Measurements, Inc., three-beam gamma densitometer
Void fraction	Auburn model 1080 conductance gage
Velocity	Flow Technology turbine meter
Momentum	Ramapo drag disk (string probe tests only)

^a0.00631 m³/sec (100 gpm) to 0.03155 m³/sec (500 gpm) Fisher-Porter electromagnetic flowmeter.

Both steady-state and transient runs were made with the string probe. Each steady-state test was approximately 15 minutes in duration, while transients of 1 min and of 30 sec were run. Two series of steady-state tests were performed. The results of the first series served as a measure

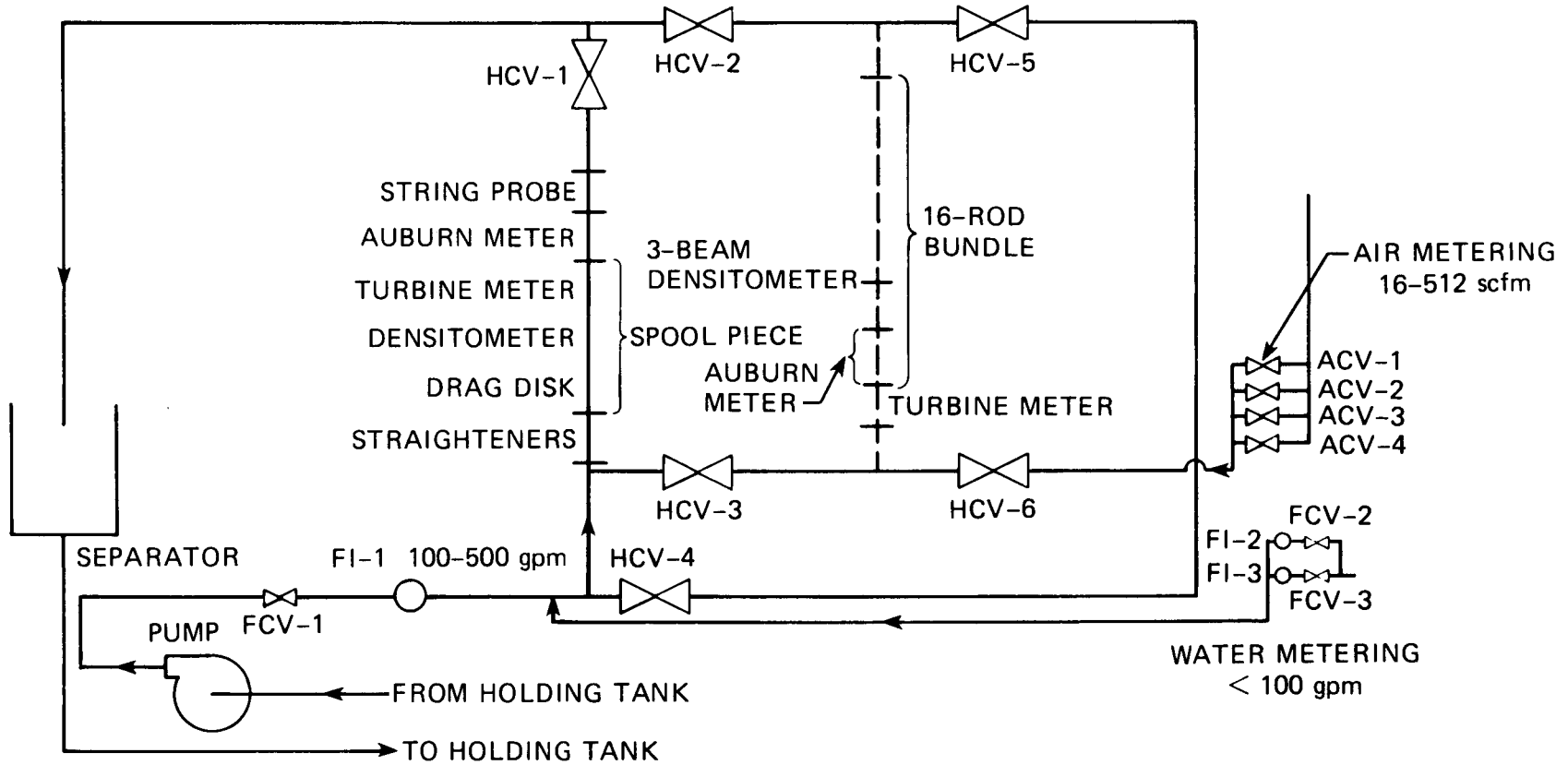


Fig. 10. Location of impedance probes in air-water test loop.

of the improvement of the quality of the results due to the improvements made in the system; the results of the second, which covered a wider range of parameters, were used to compare the velocities obtained from standard noise-analysis techniques to those obtained by the cross-correlation algorithm. In addition, these runs represented steady-state points over the entire range of parameters covered during the transients. The measured air and water flow rates and their resultant void fractions (as measured by the Auburn meter and gamma densitometer for String Probe Test Series I and II) are shown in Tables 3 and 4. For the transient tests, the initial flow conditions were $0.0680 \text{ m}^3/\text{sec}$ (144 scfm) of air and $0.0063 \text{ m}^3/\text{sec}$ (100 gpm) of water. In a transient run the procedure was to manually close the air inlet valve at such a rate as to maintain a constant rate of change in void fraction (as measured by the gamma densitometer). Two transient runs were analyzed. In the first case, the air flow rate was varied from $0.0680 \text{ m}^3/\text{sec}$ (144 scfm) to $0 \text{ m}^3/\text{sec}$ in 1 min; in the second case, the same flow rate variation took place in 30 sec. While these were the changes occurring in the flow rate at the air metering station, damping and lag occurring in the system resulted in a delayed occurrence of these conditions at the string probe location.

5.2 Results and Analysis - Steady-State Runs

Steady-state noise-analysis results indicate significant improvement in the quality of the data obtained over that of those previously reported results.⁴ Figures 11 and 12 (taken from runs 1 and 18 of Series II, which were made at void fractions of 0.103 and 0.723, respectively) indicate a

Table 3. Steady-state air and water flow rates and their void fractions for Test Series I

Test No.	Air flow		Water flow		Void fraction	
	m ³ /sec	(scfm)	m ³ /sec	(gpm)	Gamma densitometer	Auburn meter
1	0.00755	(16)	0.0252	(400)	0.185	0.181
2	0.00755	(16)	0.0063	(100)	0.375	0.434
3	0.0236	(50)	0.0063	(100)	0.595	0.750
4	0.0472	(100)	0.0063	(100)	0.715	0.891
5	0.0944	(200)	0.0063	(100)	0.838	0.956
6	0.1416	(300)	0.0063	(100)	0.885	0.980
7	0.1888	(400)	0.0063	(100)	0.907	0.991
8	0.2265	(480)	0.0063	(100)	0.914	0.995
9	0.2265	(480)	0.0032	(50)	0.956	0.999
10	0.2265	(480)	0.0013	(20)	0.974	0.999

Table 4. Steady-state air and water flow rates and their void fractions for Test Series II

Test No.	Air flow		Water flow		Void fraction	
	m ³ /sec	(scfm)	m ³ /sec	(gpm)	Gamma densitometer	Auburn meter
1	≈0.00378	(≈8)	0.0252	(400)	0.103	0.124
2	≈0.00283	(≈6)	0.0189	(300)	0.139	0.108
3	0.00755	(16)	0.0252	(400)	0.165	0.212
4	0.00755	(16)	0.0189	(300)	0.221	0.300
5	0.0142	(30)	0.0189	(300)	0.318	0.582
6	≈0.00378	(≈8)	0.0032	(50)	0.354	0.341
7	0.0236	(50)	0.0189	(300)	0.391	0.728
8	0.00755	(16)	0.0063	(100)	0.402	0.513
9	0.0354	(75)	0.0189	(300)	0.469	0.842
10	0.00755	(16)	0.0032	(50)	0.492	0.506
11	0.0472	(100)	0.0189	(300)	0.518	0.866
12	0.0142	(30)	0.0063	(100)	0.545	0.714
13	0.0142	(30)	0.0032	(50)	0.594	0.641
14	0.0236	(50)	0.0063	(100)	0.626	0.815
15	0.0236	(50)	0.0032	(50)	0.643	0.734
16	0.0354	(75)	0.0063	(100)	0.679	0.884
17	0.0354	(75)	0.0032	(50)	0.679	0.822
18	0.0422	(100)	0.0063	(100)	0.723	0.925
19	0.0472	(100)	0.0032	(50)	0.776	0.882
20	0.0708	(150)	0.0063	(100)	0.784	0.958
21	0.0944	(200)	0.0063	(100)	0.819	0.975
22	0.0708	(150)	0.0032	(50)	0.841	0.964

strong linearity in the phase angle of the transfer function of the X-, Y-probe combination over the entire range of results. Thus the proximity of the bend in the piping system can be regarded as the most probable cause of the nonlinearity in the phase angle in the previously reported⁴ test results.

In most other respects, the results are very similar to those obtained in Test Series I. At low void fractions, signal levels, presented in the

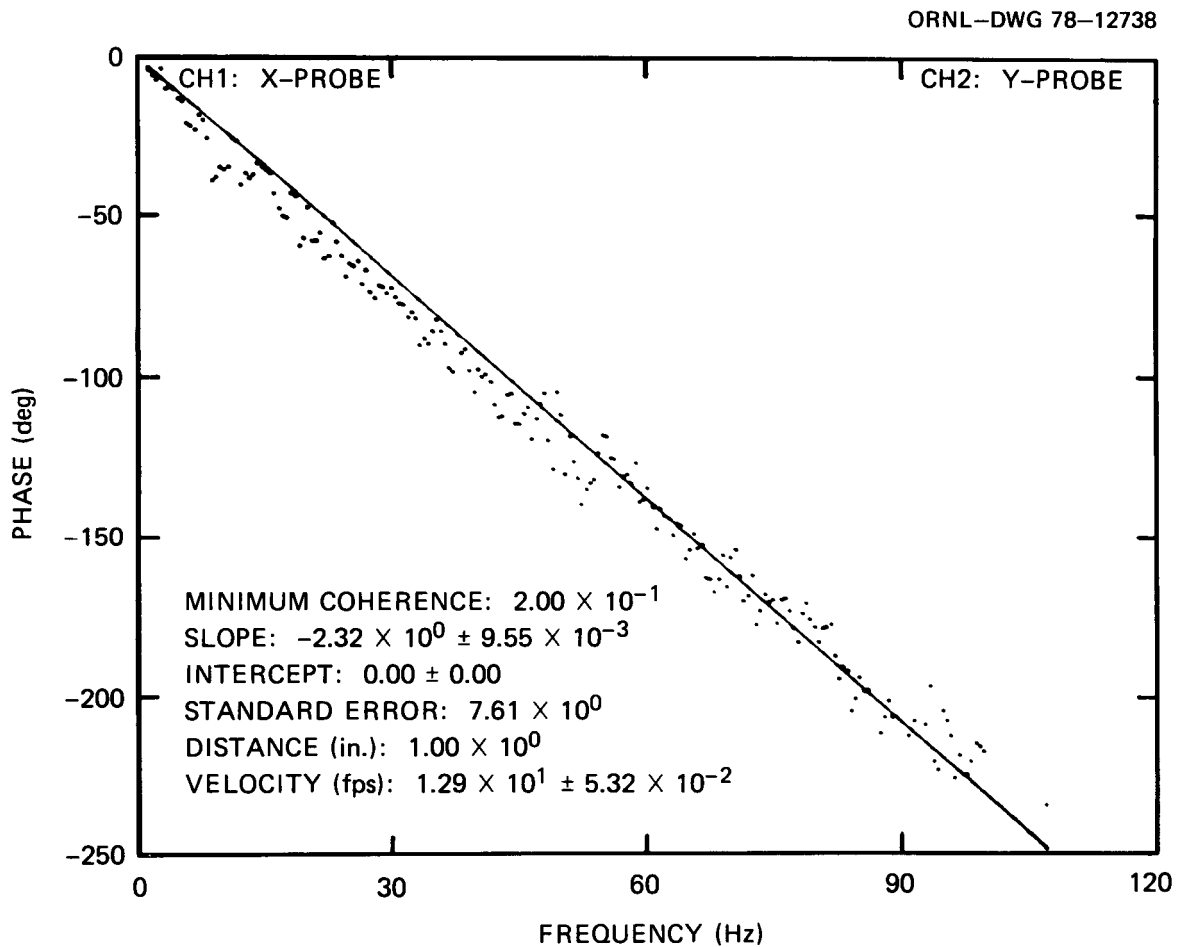


Fig. 11. Phase angle results from string probe at a void fraction of 0.103; air-water steady-state Series II.

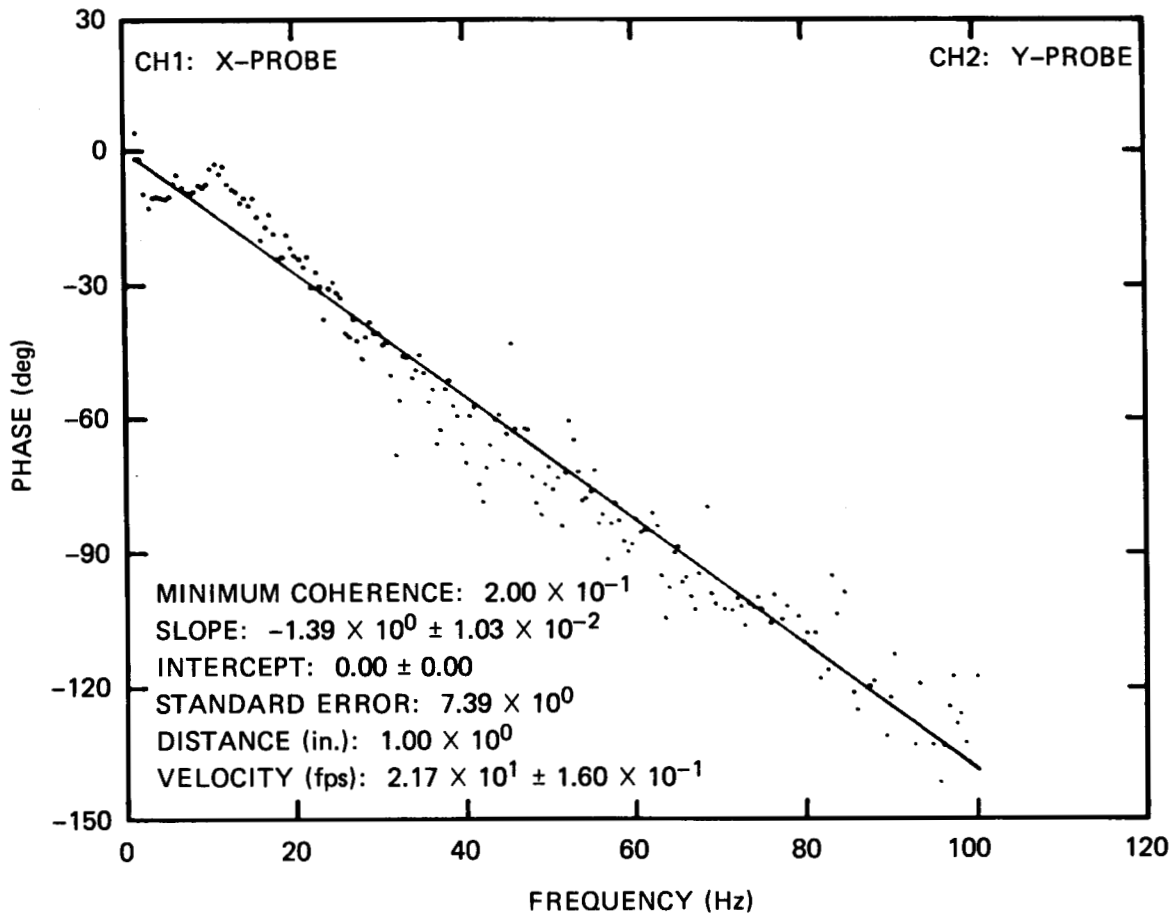


Fig. 12. Phase angle results from string probe at a void fraction of 0.732; air-water steady-state Series II.

form of power spectral densities (Fig. 13), are considerably higher than background noise levels ($10^{-8} \text{ V}^2/\text{Hz}$). In addition, a high coherence level is noted (Fig. 14) over a wide range of frequencies (≈ 0 to 80 Hz).

However, the power spectral densities obtained at very high void fractions are indistinguishable from background noise and the coherences are less than 0.1

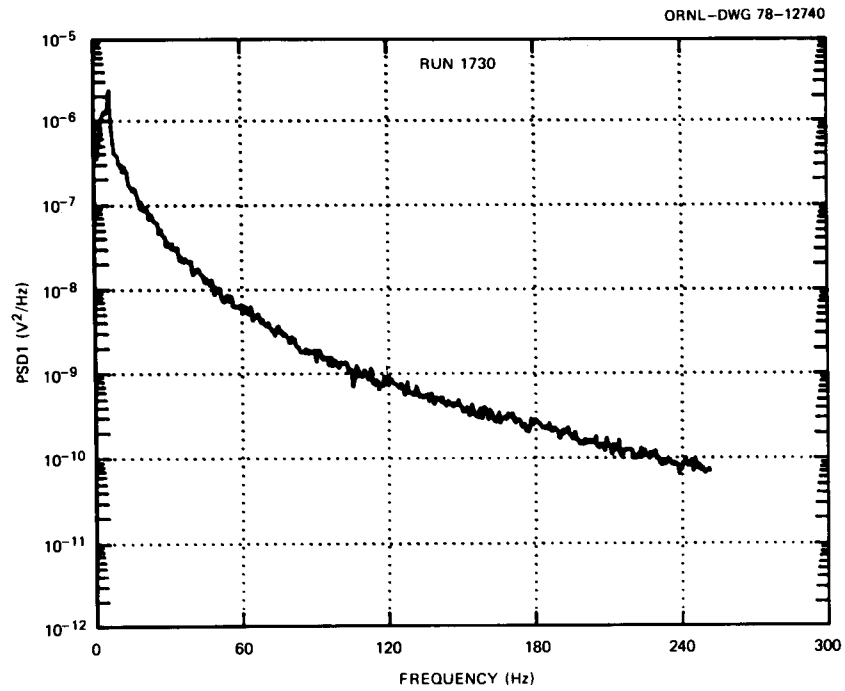


Fig. 13. Power spectral density (PSD) levels vs frequency at a void fraction of 0.42; air-water steady-state Series II.

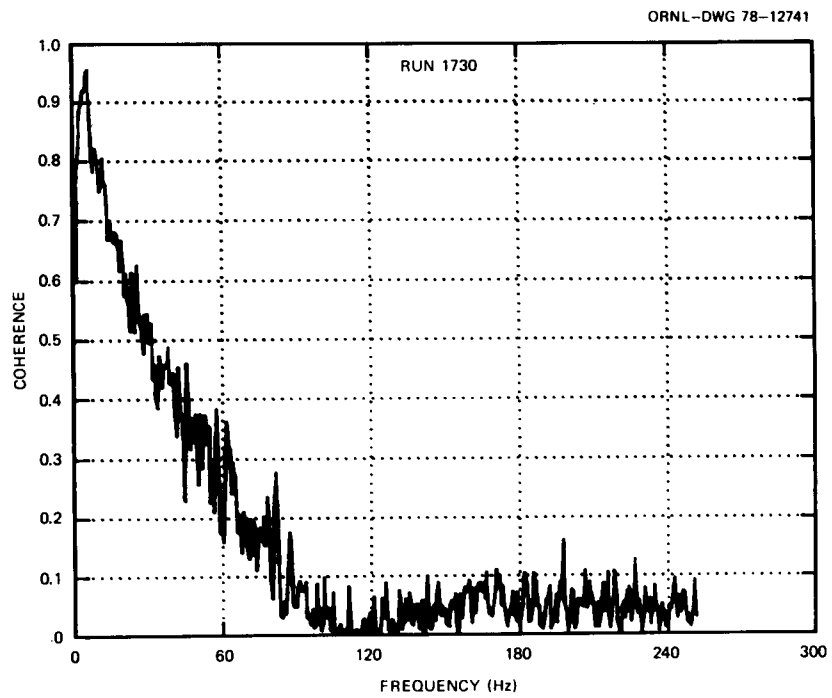


Fig. 14. Coherence level vs frequency at a void fraction of 0.42; air-water steady-state Series II.

The following equation is used to obtain slip velocities from the quality and void fraction:

$$\frac{1 - \chi}{\chi} = \frac{V_f}{V_g} \frac{\rho_f}{\rho_g} \frac{1 - \alpha}{\alpha}, \quad (5.1)$$

where χ is the quality, ρ is the density, V is the velocity, and α is the void fraction. The subscripts f and g refer to the liquid and vapor phases, respectively. When Eq. (5.1) is coupled with the continuity equation

$$\dot{m} = \rho_f(1 - \alpha) AV_f + \rho_g \alpha AV_g, \quad (5.2)$$

the unknown velocities can be solved. In this equation, it is assumed that all the liquid is moving at the same velocity, V_f , and all the vapor is moving at velocity V_g .

The void fractions listed in Tables 3 and 4 show a difference between the measured values of the gamma densitometer and the Auburn conductance meter, with the Auburn meter readings consistently higher. Because the relationship between conductance and void fraction is not necessarily linear (as noted by Merit et al.⁵) and because of the previously noted⁶ uncertainty of the Auburn meter output at high void fraction, the gamma densitometer void fraction values were chosen as reference values for the results reported here. In addition, a comparison was also made with several slip velocity models in the literature. The models, which have been described previously,⁴ are the Govier and Aziz⁷ model, the Hughmark and Pressburg⁸ model, Hughmark's modification to the Bankoff⁹ model, and the homogeneous model. For Test Series I, the calculated liquid and vapor velocities and the velocity obtained from noise-analysis techniques are

given in Table 5. As can be seen in this table, use of the gamma densitometer void fraction yields liquid and vapor velocities that are in close agreement with the various slip velocity models over the entire void fraction range.

By comparing the velocity obtained from noise-analysis techniques with that derived from the measured liquid and vapor flow rates and the gamma densitometer readings, the following conclusions may be drawn:

1. At low void fractions ($\alpha \lesssim 0.40$), the noise-analysis velocity estimate is close to V_g .
2. At intermediate void fractions ($0.40 \lesssim \alpha \lesssim 0.80$), the noise-analysis velocity estimate is less than the liquid velocity.

This trend should not be too surprising. Since noise-analysis techniques tend to correlate signal fluctuations, the negative spikes occurring at low void fractions are caused by bubbles; therefore, the correlation of the fluctuations would necessarily yield a velocity close to that representing the vapor velocity. At intermediate void fractions, alternating positive and negative spikes representing slugs of water and vapor, respectively, tend to yield a velocity intermediate to the two phase velocities. At very high void fractions, where the vapor phase is continuous, the correlated position spikes are caused by the liquid droplets. In this last case, it is important to point out that in air-water testing the annular mist flow regime may be predominant and the velocity measured could possibly be that of the film on the wall rather than the droplets in the mist. Thus, in this case, air-water tests would not be representative of what the string probe would encounter in the upper plenum of a reflood test facility.

Table 5. Comparison of calculated liquid and vapor velocities with the velocity determined by standard noise-analysis techniques for String Probe Test Series I steady-state runs

Model ^a	Run No.									
	1	2	3	4	5	6	7	8	9	10
Auburn meter										
V _f	12.5	4.5	10.2	23.5	58.1	130.3	293.8	485.0	10392.	7782.
V _g	16.9	7.0	12.7	21.4	40.0	58.4	77.1	92.2	91.7	91.7
α	0.181	0.434	0.750	0.891	0.956	0.980	0.991	0.995	0.9998	0.9999
Gamma densitometer										
V _f	12.6	4.1	6.3	9.0	15.7	22.2	27.3	29.8	29.2	20.0
V _g	16.5	8.1	16.0	26.7	45.6	64.7	84.3	100.2	95.9	94.1
α	0.185	0.375	0.595	0.715	0.838	0.885	0.907	0.914	0.956	0.974
Govier and Aziz ⁷										
V _f	12.7	4.3	6.7	8.9	11.1	14.5	18.4	20.9	21.9	10.7
V _g	15.8	7.4	15.4	26.8	49.8	69.6	89.1	104.5	142.1	96.4
α	0.193	0.413	0.619	0.714	0.769	0.824	0.861	0.878	0.944	0.952
Hughmark and Pressburg ⁸										
V _f	12.6	4.6	6.7	8.5	10.7	12.7	15.0	16.5	10.2	6.4
V _g	16.1	6.9	15.4	27.3	50.3	71.6	92.0	108.4	104.7	99.7
α	0.19	0.44	0.620	0.70	0.76	0.80	0.83	0.845	0.875	0.920
Hughmark modification to Bankoff ⁹										
V _f	12.5	4.3	6.8	8.7	10.2	11.3	19.8	20.6	11.4	6.01
V _g	17.0	7.5	15.3	27.1	50.9	73.9	87.8	105.0	103.2	100.3
α	0.18	0.409	0.623	0.706	0.75	0.775	0.871	0.876	0.888	0.915
Homogeneous										
Velocity	13.3	5.62	12.1	21.6	40.5	59.4	79.8	94.6	93.2	92.2
α	0.23	0.545	0.789	0.882	0.937	0.957	0.968	0.973	0.986	0.995
Noise analysis	<i>b</i>	6.99	11.9	17.8	8.8	10.8	8.8	7.9	<i>c</i>	<i>c</i>
Frequency range analyzed, Hz		0-20	0-20	0-40	0-10	0-20	0-20	0-20		

^a V_f = liquid velocity (in feet per second); V_g = vapor velocity (in feet per second); α = void fraction.

^b No noise-analysis results for run no. 1.

^c Signal level was too low and coherence too poor to obtain a meaningful velocity.

The noise-analysis results from Test Series II were reduced using both standard noise-analysis techniques and the adaptive cross-correlation algorithm. Different frequency ranges were analyzed depending on the shape of the coherence curve. If the coherence remained high, the range of 0-100 Hz was generally analyzed; for cases where the coherence decreased rapidly with increased frequency, only the range where meaningful coherence (usually greater than ≈ 0.1) existed was analyzed. The analysis results are given in Table 6.

The conclusions reached from the analysis of the Series II runs are similar to those from Series I. At low void fractions, noise-analysis velocities similar to the vapor velocity are obtained. As the void fraction is increased, velocity predicted by noise analysis deviates further from the vapor velocity and approaches that of the liquid; however, some runs do not follow this trend. One reason for this difference may be the frequency range over which the data were analyzed. In Series I, the data were analyzed over the frequency range of 0-20 Hz; in Series II, this range was varied. The bases for frequency range selection are not known at this time. Factors such as coherence may be important in this selection, while another explanation for the discrepancy lies in the string probe itself. After the completion of Series II, the string probe was removed from the test loop, and it was noted that two wires in the Y-plane and one in the X-plane were broken. It is not known when this occurred, but it was sometime during the Series II runs.

Since the function of these instruments is to measure liquid flow rates, a knowledge of the liquid velocity is important. It is suggested that the following assumptions and technique be employed to determine the liquid velocity.

Table 6. Comparison of calculated liquid and vapor velocities with the velocity determined by standard noise analysis techniques and the adaptive cross-correlation algorithm for String Probe Test Series II steady-state runs

Run No.	Gamma densitometer data results			Govier and Aziz ⁷		V homogeneous (fps)	Noise-analysis velocity ^a (fps)	Frequency range analyzed (Hz)	Adaptive cross-correlation algorithm velocity (fps)
	α	V _g (fps)	V _f (fps)	V _g (fps)	V _f (fps)				
1	0.103	14.9	11.4	13.5	11.5	11.7	12.9 ± 0.05	0-100	13.3 ± 0.75
2	0.139	8.3	8.9	10.74	8.58	9.9	10.8 ± 0.03	0-100	11.0 ± 0.7
3	0.165	18.6	12.2	16.2	12.6	13.3	14.4 ± 0.04	0-100	14.2 ± 0.9
4	0.221	13.8	9.8	14.6	9.7	11.3	12.2 ± 0.03	0-100	12.0 ± 0.7
5	0.318	18.0	11.2	18.1	11.3	14.0	14.2 ± 0.42	0-100	14.3 ± 0.9
6	0.354	4.3	2.0	3.4	2.3	2.8	5.54 ± 0.07	0-20	8.6 ± 7.0
7	0.391	24.4	12.6	22.5	13.5	17.8	14.0 ± 0.16	0-30	17.3 ± 1.5
							16.6 ± 0.07	0-100	
8	0.402	7.6	4.3	7.28	4.4	5.6	8.08 ± 0.57	0-40	8.7 ± 2.0
9	0.469	30.5	14.4	28.3	15.5	22.5	21.4 ± 0.13	0-100	21.1 ± 1.3
10	0.492	6.2	2.5	5.5	2.9	4.3	7.23 ± 0.09	0-35	10.3 ± 10.0
11	0.518	36.8	15.9	34.7	17.0	27.3	20.3 ± 0.12	0-50	24.0 ± 3.4
12	0.545	10.5	5.6	10.7	5.6	8.4	10.6 ± 0.60	0-60	11.4 ± 1.2
13	0.594	9.7	3.1	9.32	3.39	7.1	8.78 ± 0.16	0-30	10.3 ± 5.0
14	0.626	15.3	6.8	15.2	6.9	12.1	13.7 ± 0.75	0-90	13.1
15	0.643	14.9	3.6	14.4	3.8	10.8	8.41 ± 0.16	0-30	9.5 ± 8.5
16	0.679	21.1	8.0	21.3	7.8	16.9	17.3 ± 0.12	0-100	17.1
17	0.679	21.1	4.0	20.4	4.3	15.6	9.64 ± 0.24	0-30	12.7 ± 10.0
18	0.723	26.4	9.2	26.8	8.9	21.7	21.7 ± 0.16	0-100	24.2
19	0.776	24.6	5.7	26.1	4.7	20.4	9.01 ± 3.04	0-25	12.5 ± 8.8
20	0.784	36.6	11.8	38.8	9.7	31.2	24.6 ± 0.23	0-100	27.7
21	0.819	46.7	14.1	49.1	11.4	40.8	29.0 ± 0.32	0-100	28.4
22	0.841	34.1	8.0	36.2	6.0	29.9	10.7 ± 0.22	0-40	10.4 ± 12.0

^a Error bands on velocities represent the standard deviation of the straight-line fit to the phase angle vs frequency curve.

1. The velocity determined from noise analysis always lies between the liquid and vapor velocities.

2. The velocity determined from noise analysis is a linear function of the void fraction. It is the same as the gas velocity at very low void fractions, the same as the liquid velocity at very high void fractions, and is a function of void fraction at intermediate void fractions. This can be written as

$$V_{\text{noise}} = (1 - \alpha) V_g + \alpha V_f. \quad (5.3)$$

In an actual reflood test, the following information is available:

α , V_{noise} , P , and T . From P and T we can determine ρ_f and ρ_g . In order to determine the relationship between V_g and V_f , we need to know the slip ratio. This can be obtained for air-water by using one of the correlations shown in Table 6. Of those, the correlation of Govier and Aziz⁷ was found to agree best with the present data. This correlation is based on knowledge of the superficial liquid and vapor velocities (V_{sf} and V_{sg}), which can be written as:

$$V_{sf} = (1 - \alpha) V_f \quad (5.4)$$

and

$$V_{sg} = \alpha V_g, \quad (5.5)$$

with

$$S = \text{slip ratio} = V_g/V_f = \frac{V_{sg}}{V_{sf}} \frac{1 - \alpha}{\alpha}. \quad (5.6)$$

Since only α and V_{noise} are known, the solution to Eqs. (5.3)–(5.6)

requires a trial-and-error solution. A slip ratio is assumed, and Eq. (5.3) is solved for V_f and V_g . These values are then plugged into Eqs. (5.4) and (5.5), and the correlation is used to obtain a new value for S . This new value is used again in Eq. (5.3) to obtain improved values for V_f and V_g . This process is repeated until the iteration yields a constant value of S . The value of V_f then represents the liquid velocity.

For the case of steam-water, several correlations for void fraction are available. They include the results of Martinelli and Nelson,¹⁰ Thom,¹¹ Bankoff,¹² and Hughmark.¹³ Of these, the Thom¹¹ correlation is relatively simple to use and has been found to yield satisfactory results for steady-state cases. It is assumed that steady-state correlations are applicable to the types of transients commonly experienced during reflood and that the flow regimes encountered are not very different; the inaccuracy associated with these assumptions is uncertain. This technique was applied to the results of Series I and II where void fractions of 0.80 or less occurred. As can be seen in Fig. 15, most of the points lie within the $\pm 30\%$ range, with most of the higher percentage deviations occurring at the lower flow rates. Further preliminary analysis indicates that the larger deviations occur at void fractions above 0.35 and in tests where the data are analyzed over a low frequency range.

5.3 Results and Analysis - Transient Runs

Because of the lag caused by the resistance in the air-water system, the instantaneous air flow rate at the test section may be significantly different from that at the air metering station. Consequently, only the instruments in the spool piece (i.e., the turbine meter, drag disk, and

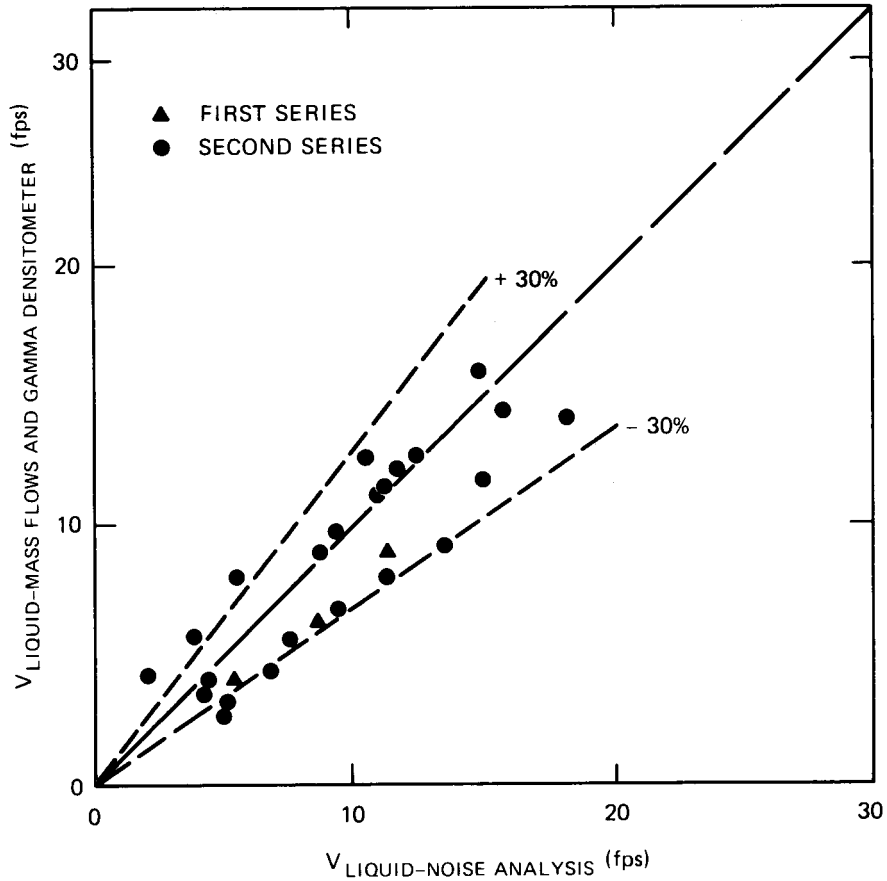


Fig. 15. Comparison of liquid velocity deduced from noise analysis using a simplified model and the liquid velocity determined from metered-in flow rates and gamma densitometer.

gamma densitometer) can be used to monitor instantaneous conditions in the string probe. For simplicity it was assumed that because of the proximity of the instrumented spool piece and the string probe, the same conditions occur at the two locations at any instant during the transient.

The void fraction profiles measured by the gamma densitometer for the 1-min and the 30-sec transients are given in Figs. 16 and 17, respectively. The void fraction gradient is not linear and, as

2 - PHASE FLOW VERTICAL UPFLOW 1 MINUTE TRANSIENT

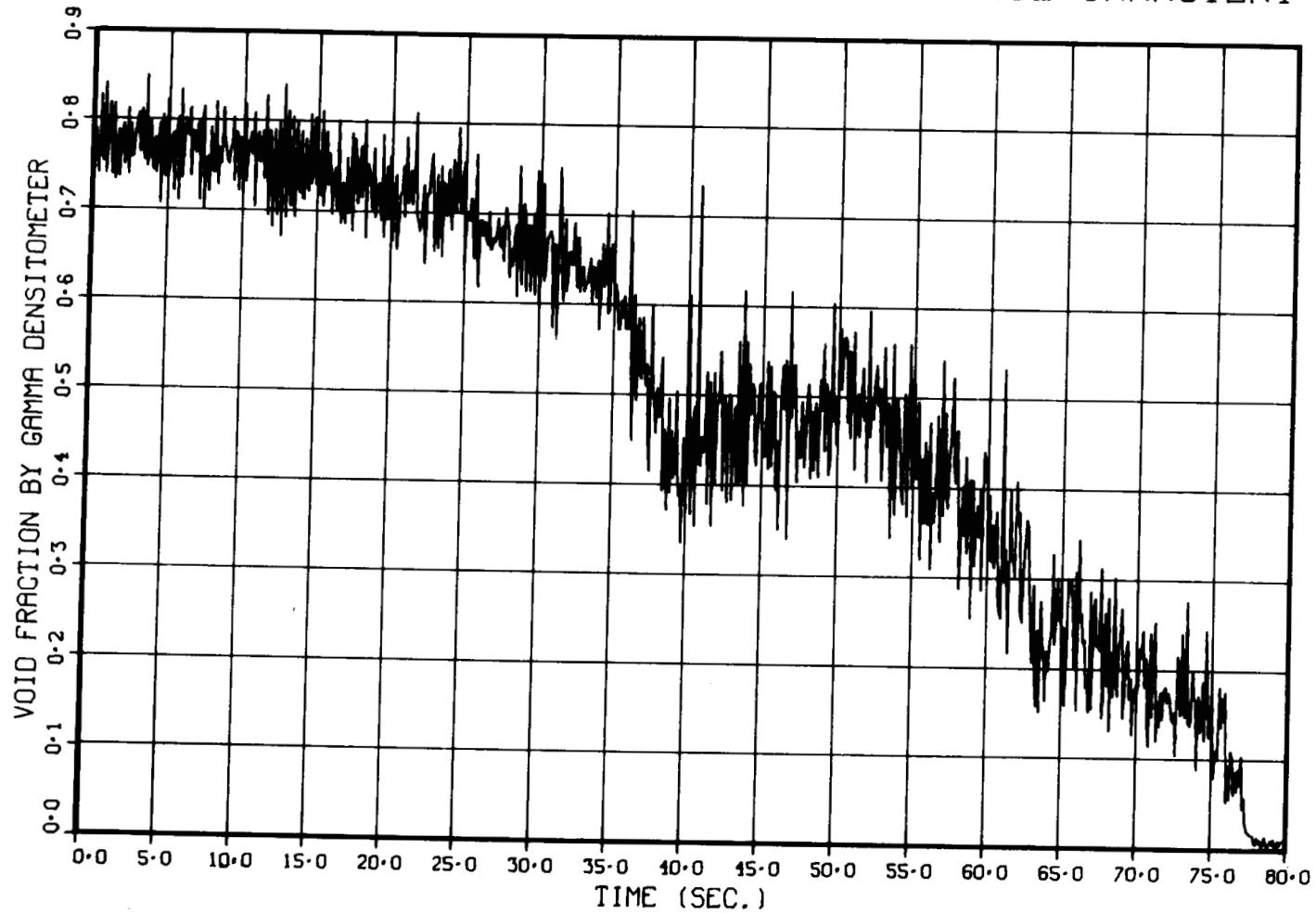


Fig. 16. Void fraction profile measured by gamma densitometer for the 1-min transient.

2 - PHASE FLOW VERTICAL UPFLOW 30 SECOND TRANSIENT

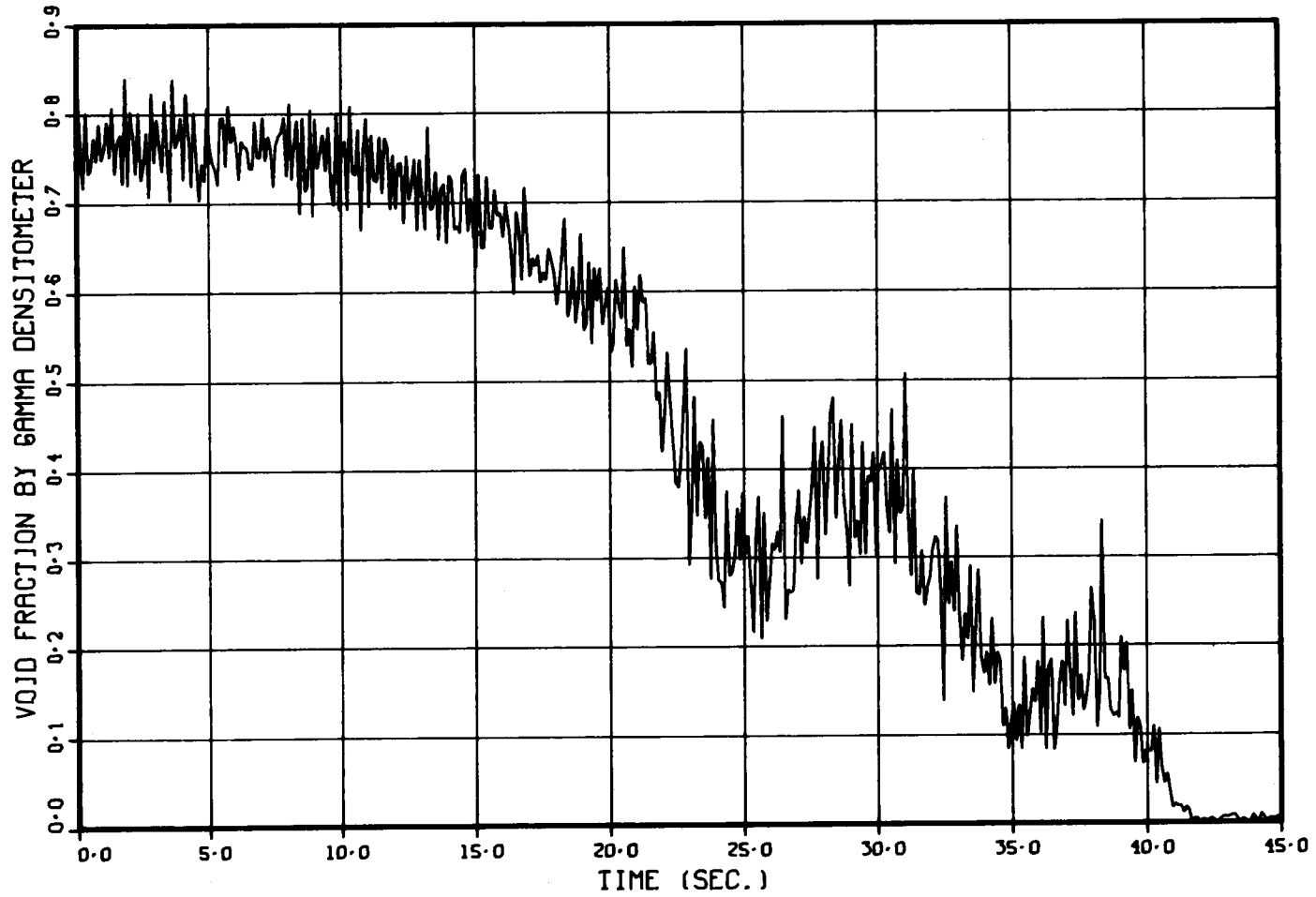


Fig. 17. Void fraction profile measured by gamma densitometer for the 30-sec transient.

previously noted, tends to lag the conditions at the air metering station. The following technique was used to determine the liquid and vapor velocities during the transient.

1. Using density (from gamma densitometer) vs time plots, as shown in Figs. 16 and 17, data points denoting Series II steady-state runs were located on this graph. For example, in the transient, the water flow was held constant at $0.0063 \text{ m}^3/\text{sec}$ (100 gpm) and the air varied from $0.0680 \text{ m}^3/\text{sec}$ (144 scfm) to zero. Therefore, the intermediate points of 100, 75, 50, 30, and 16 scfm which were tested in Series II were located on the density vs time curve by matching the densities on the graph with the density recorded by the gamma densitometer for these steady-state runs.

2. As a further check on the location of the steady-state runs on the transient curve, a plot of turbine meter velocity vs time was used to locate the steady-state conditions. In all cases, the points determined from the gamma densitometer agreed with those from the turbine meter within approximately 1 sec. This difference appears reasonable in light of the manual technique used for time correlation.

3. The corresponding liquid and vapor velocities associated with each point as determined from metered in-flow rates and the three-beam gamma densitometer were noted.

4. During the recording of string probe signals on tape, the turbine meter and "B" beam gamma densitometer voltages were recorded simultaneously on adjacent channels of the 14-track tape recorder and on the computer-based data acquisition system (DAS) used to record the two-phase data. It could not be assumed with certainty that the start of the two-phase

flow data recording on the DAS coincided with that of the noise analysis recording on the tape recorder, but a comparison of turbine meter voltages and "B" beam signals from the two different data recording systems made it possible to exactly match the events in time to an acceptable tolerance.

5. The liquid and vapor velocity curves determined from the Aya model were examined. Although the magnitude of the vapor and liquid velocities obtained by the model could not be assumed to be accurate over the wide range of conditions tested here,^{14,15} the shapes of the curves were assumed to be more dependable. Curves were then fitted through the points representing the liquid and vapor velocities as a function of time, with the curves' shape resembling that of the Aya model. Figures 18 and 19

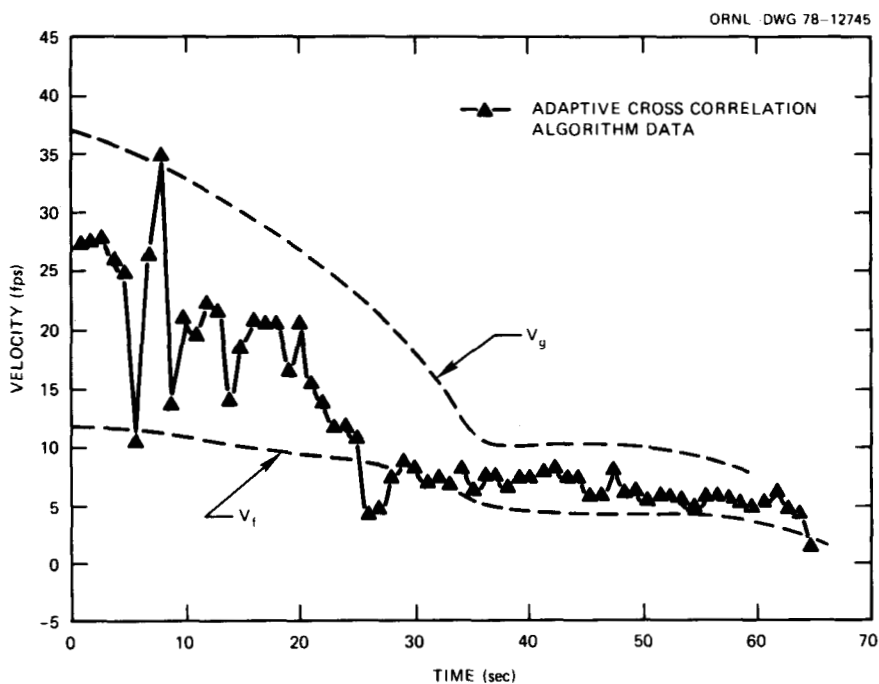


Fig. 18. Comparison of noise-analysis velocity obtained from adaptive cross-correlation algorithm with the liquid and vapor velocities obtained from two-phase flow instruments - 1-min transient.

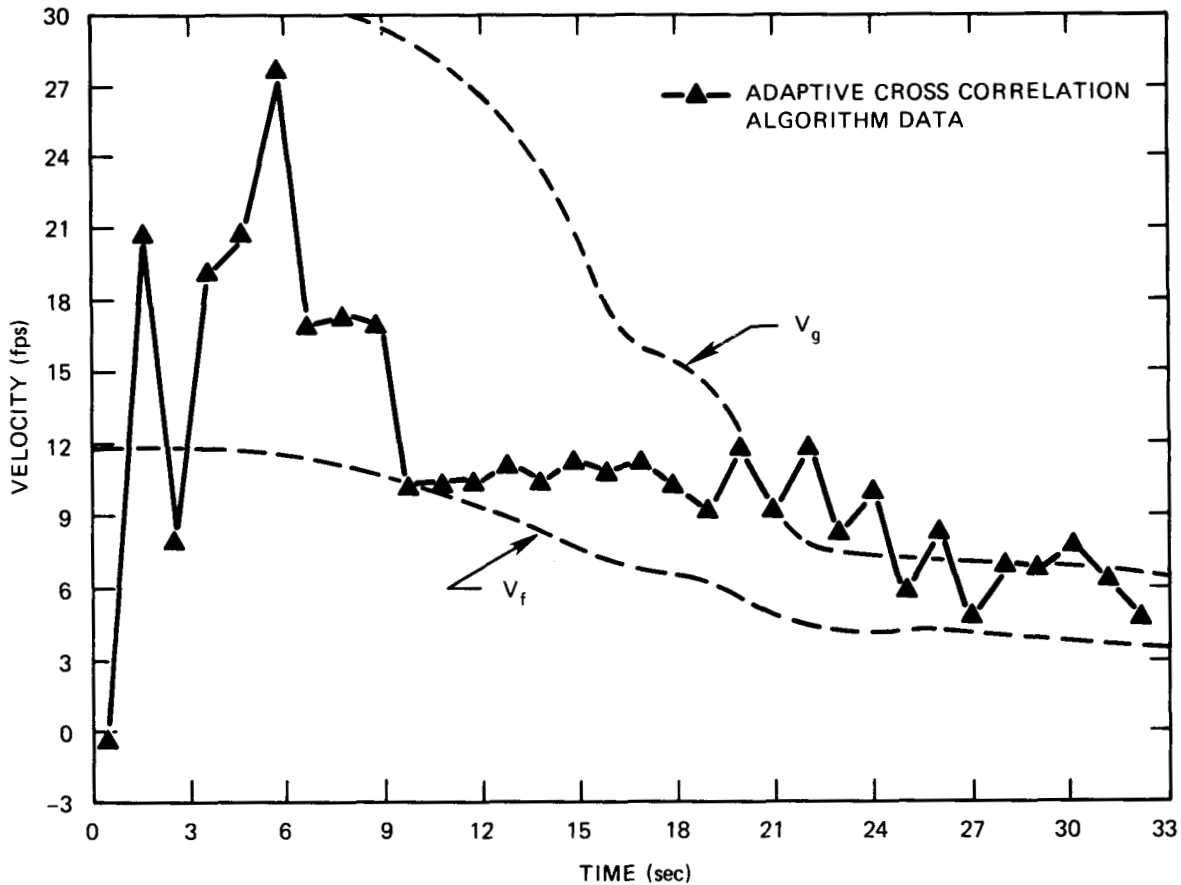


Fig. 19. Comparison of noise-analysis velocity obtained from adaptive cross-correlation algorithm with the liquid and vapor velocities obtained from two-phase flow instruments - 30-sec transient.

are the plots obtained for the 1-min and the 30-sec transients, respectively. Note that in most cases, the velocity obtained by the adaptive cross-correlation algorithm lies in between the liquid and vapor velocities. In Figs. 18 and 19, the velocity determined by the adaptive cross-correlation algorithm does not exhibit the smooth trend obtained from the two-phase flow results, possibly because the algorithm traced some of the slugs occurring in the flow.

6. STRING PROBE VOID FRACTION MEASUREMENT

W. H. Andrews P. A. Jallouk*
J. E. Hardy* W. H. Leavell

6.1 Testing Procedure

Void fraction measurements were made with the string conductance probe in the two-phase air-water facility in the vertical upflow mode. Void fractions were determined by powering the string probe with an ac voltage and measuring the voltage drop across a precision resistor in series with the probe. The electric circuit was designed so that the voltage drop was linearly proportional to the conductivity of the two-phase mixture in the string probe; the conductivity of the mixture was then assumed to be linearly proportional to the void fraction.

In this case, as in the velocity readings, a water conductivity of at least 80 μS had to be maintained for the electronic circuit to function properly. All runs were made with readings of 140–160 μS .

6.2 Data Reduction and Analysis

A series of tests was conducted in which the average void fraction in the pipe cross section was determined for both the X- and Y-planes of the string probe. These average void fractions were compared with the results of the gamma densitometer and the Auburn meter, and the test results are listed in Table 7. Four or five tests were performed at each run number, and the void fraction listed for each instrument represents a final average. Deviation from the average value for each run was ~20%, demonstrating the reproducibility of the experiments. As

*Engineering Technology Division.

Table 7. Void fractions as measured by the string
conductance probe, gamma densitometer, and
Auburn conductance meter

Run No.	Air flow		Water flow		Void fraction			
	[m ³ /sec	(scfm)]	[m ³ /sec	(gpm)]	X-plane	Y-plane	Gamma	Auburn
1	≈0.00188	(≈4)	0.0252	(400)	0.075	0.105	0.049	0.050
2	≈0.00378	(≈8)	0.0252	(400)	0.17	0.21	0.11	0.14
3	0.00755	(16)	0.0252	(400)	0.18	0.20	0.17	0.24
4	0.00755	(16)	0.0189	(300)	0.22	0.23	0.24	0.25
5	0.00755	(16)	0.0063	(100)	0.32	0.35	0.36	0.49
6	0.0113	(24)	0.0063	(100)	0.39	0.40	0.45	0.61
7	0.0151	(32)	0.0063	(100)	0.50	0.52	0.51	0.69
8	0.0302	(64)	0.0063	(100)	0.69	0.67	0.64	0.84
9	0.1208	(256)	0.0063	(100)	0.90	0.93	0.84	0.97
10	0.2416	(512)	0.0063	(100)	0.94	0.96	0.92	0.996

shown in Table 7, the string and conductance probe's X- and Y-planes agreed with each other very well through the void fraction range tested; the probe results also matched well with the void fraction determined by the three-beam gamma densitometer. The Auburn meter readings consistently measured a higher void fraction than that of the gamma densitometer and, except for Runs 1 and 2, higher than that of the string conductance probe. A plot of the void fraction determined from the string probe vs that measured by the gamma densitometer is shown in Fig. 20.

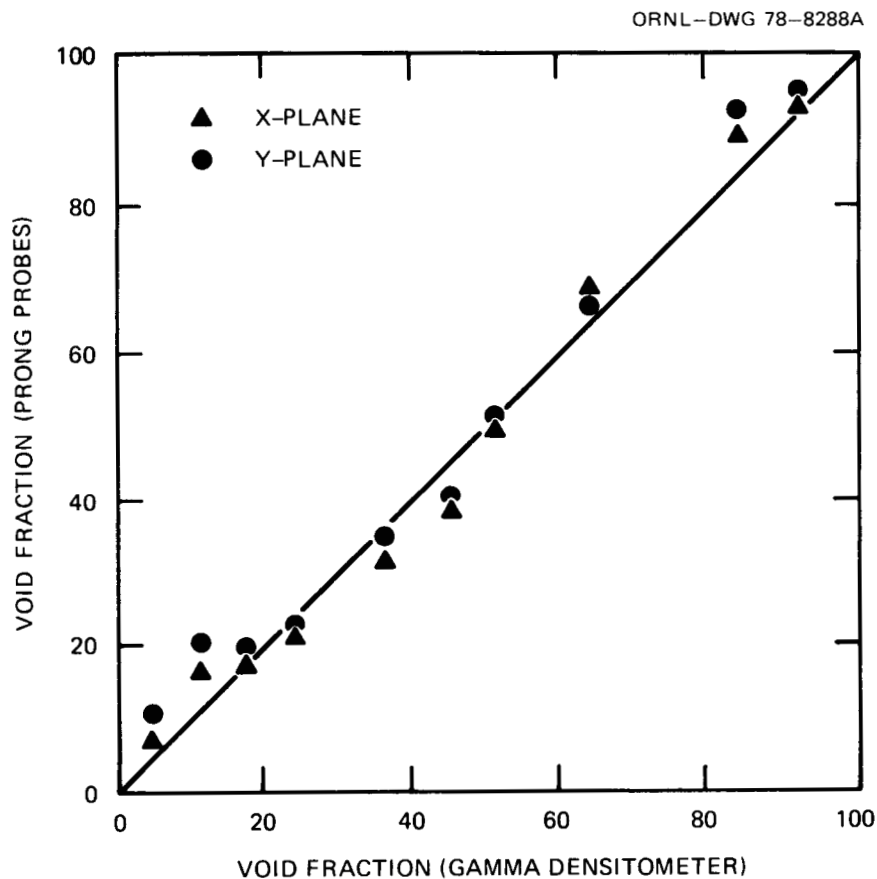


Fig. 20. Comparison of void fraction determined by string probe conductance with void fraction determined by gamma densitometer.

7. IN-BUNDLE PROBE VELOCITY MEASUREMENT

J. E. Hardy* P. A. Jallouk*
M. B. Herskovitz W. H. Leavell

7.1 Testing Procedure

In addition to string probes suitable for upper plenum measurements, a variety of probes that might be suitable for in-bundle application are being considered for testing in two-phase flow in order to deduce the liquid and vapor velocity by using noise-analysis techniques. Several types of probes used in air-water Test Bundle 1 are shown in Fig. 21.

1. Band probes. These probes consist of two bands on adjacent tubes and can be used to obtain readings across a subchannel. By using two pairs spaced a known distance apart, it may be possible to cross-correlate the signals.
2. Two-wire prong probes. These work on the same principle as the string probe described above; however, the reading is considerably more localized. The prongs extend diagonally across a subchannel to a point very close to the adjacent rod, thereby sampling a large fraction of the subchannel.
3. Four-wire prong probe. These work on the same principle as the two-wire prong probe. Of the four wires in a plane, the first and third wires form one lead, while the second and fourth form the other. A higher signal level is expected to be obtained with the four-wire probe than with the two-wire probe.

* Engineering Technology Division.

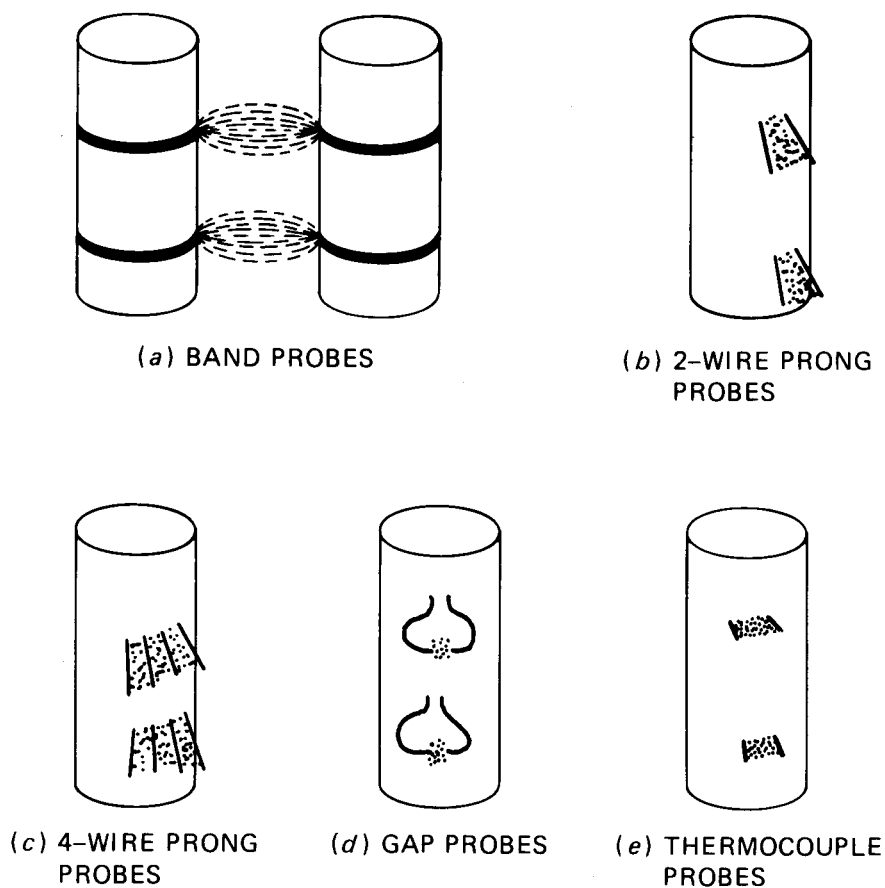


Fig. 21. Schematic diagram of various in-bundle impedance sensor configurations.

4. Gap probe. These probes protrude into the subchannel to such a point that the two tips of the wires are approximately in the center of the subchannel. The wires are insulated along their length with only the tips exposed. For this case, a distance of 1.588 mm (1/16 in.) was chosen to separate the two tips; other experimenters who have used a similar device have chosen a wide variety of spacings.

5. Thermocouple probes. These are similar to the two-wire prong probes but extend only 3.176 mm (1/8 in.) into the subchannel. They are made from thermocouple wire rather than copper.

Sketches of the locations in Bundle 1 of the various types of probes on each rod are shown in Figs. 22 through 24. The two-wire prong probes were all 25.4 mm (1 in.) apart in the axial direction, while each of the two pairs of wires in each plane was parallel and 3.175 mm (1/8 in.) apart. Correlations were attempted between levels 1 and 2, between levels 2 and 3, and between levels 3 and 4.

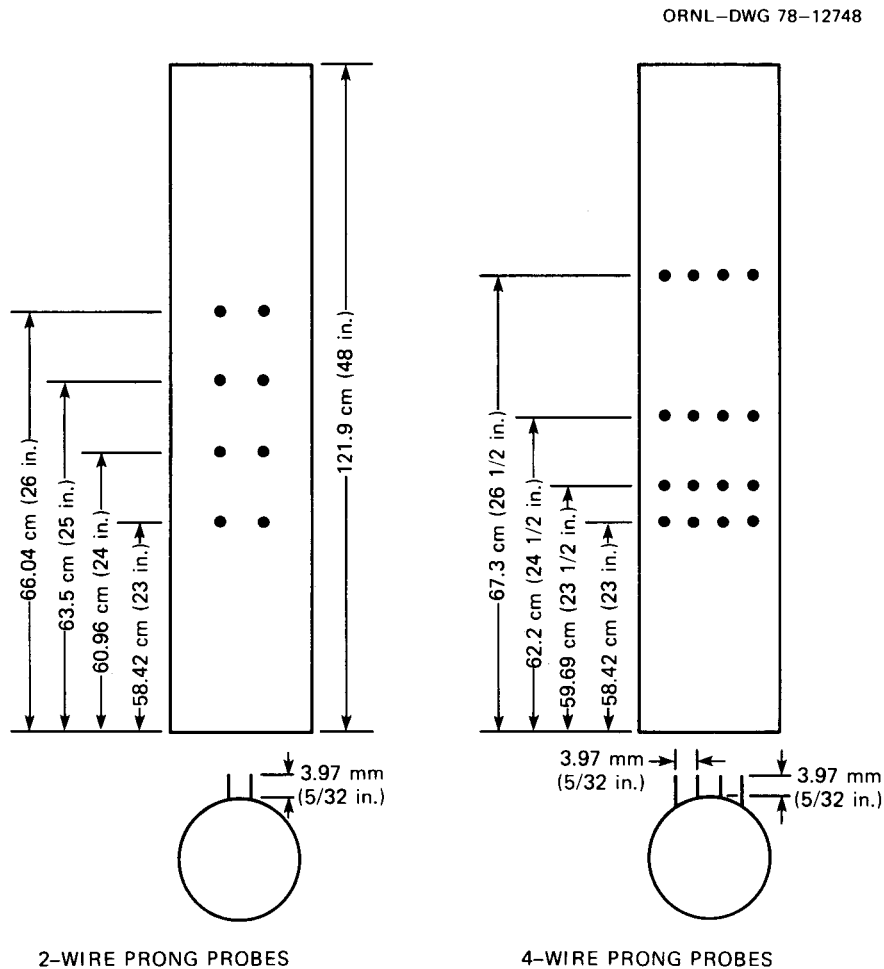


Fig. 22. Details of various instrumented rods tested in Bundle 1 (2- and 4-wire prong probes).

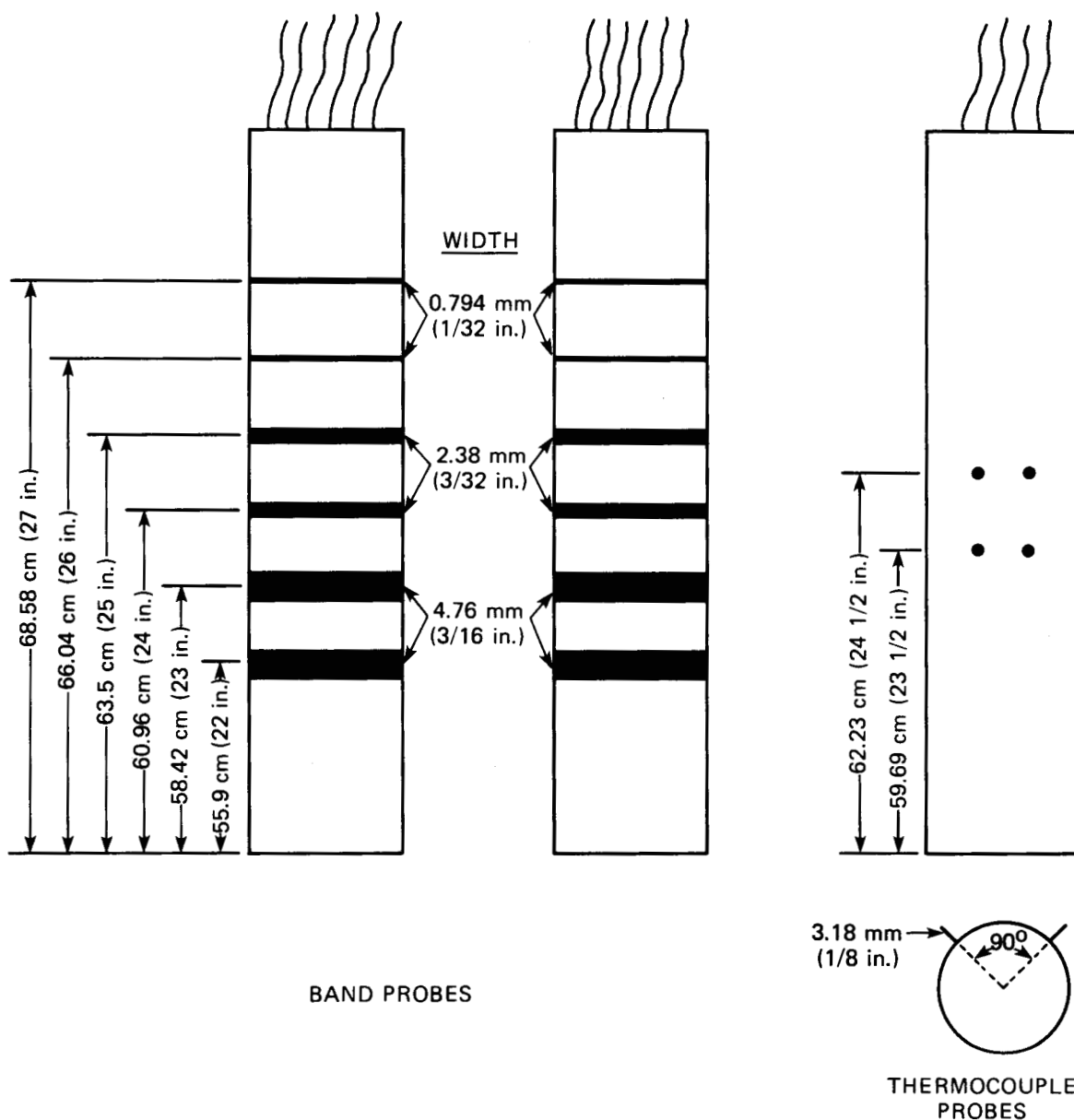


Fig. 23. Details of various instrumented rods tested in Bundle 1 (band and thermocouple probes).

The four-wire prong probes were located in four levels, each a different distance apart. It was therefore possible to determine the effect of probe distance on the coherence and accuracy of the noise-analysis signals obtained. Levels 1 and 2 were 50.8 mm (2 in.) apart,

ORNL-DWG 78-12750

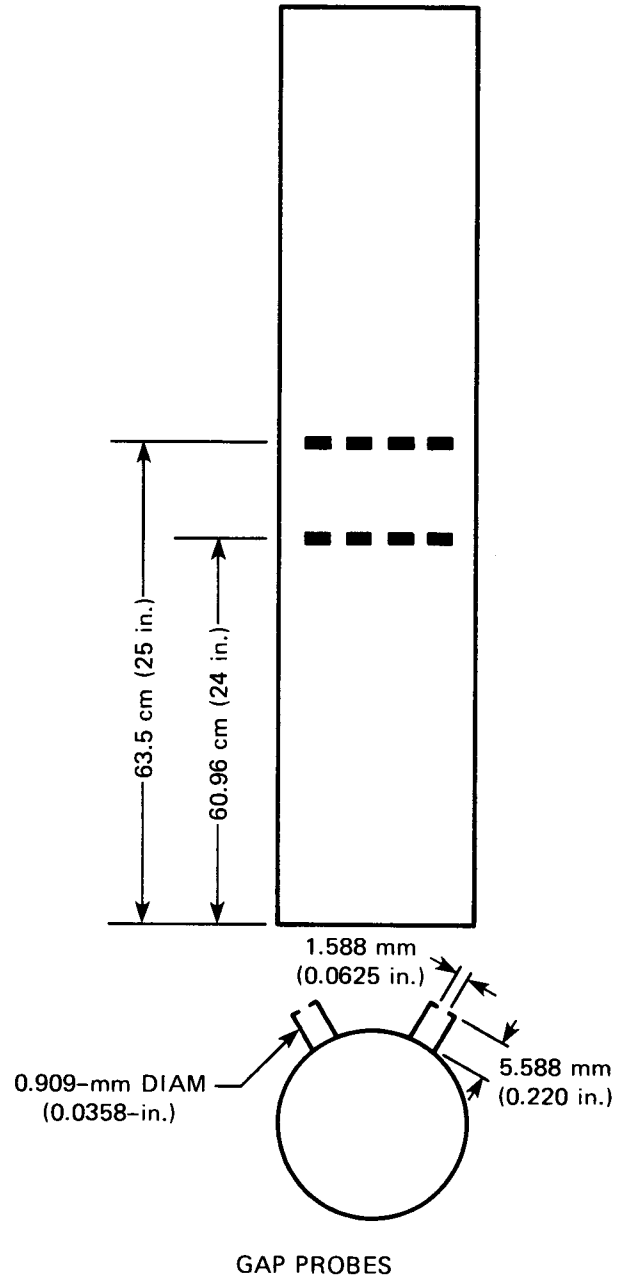


Fig. 24. Details of various instrumented rods tested in Bundle 1 (gap probes).

levels 2 and 3 were 2.54 cm (1 in.) apart, and levels 3 and 4 were 12.7 mm (1/2 in.) apart.

The band probes were all 25.4 mm (1 in.) apart from center to center, but the width of the bands varied. Those at levels 1 and 2 were 0.794 mm (1/32 in.) wide, while those at levels 3 and 4 were 2.38 mm (3/32 in.) wide, and those at levels 5 and 6 were 4.76 mm (3/16 in.) wide. Only signals from bands of the same width were cross-correlated. These bundle impedance probes were placed in a 16-rod bundle and arranged as shown in Fig. 25. The unmarked rods in Fig. 25 were made of solid Plexiglas; all were 12.7 mm (1/2 in.) in diameter and 121.9 cm (48 in.) in length. They were arranged in a sequence array with a center-to-center distance between rods of 16.93 mm (0.667 in.); thus, this bundle represented a

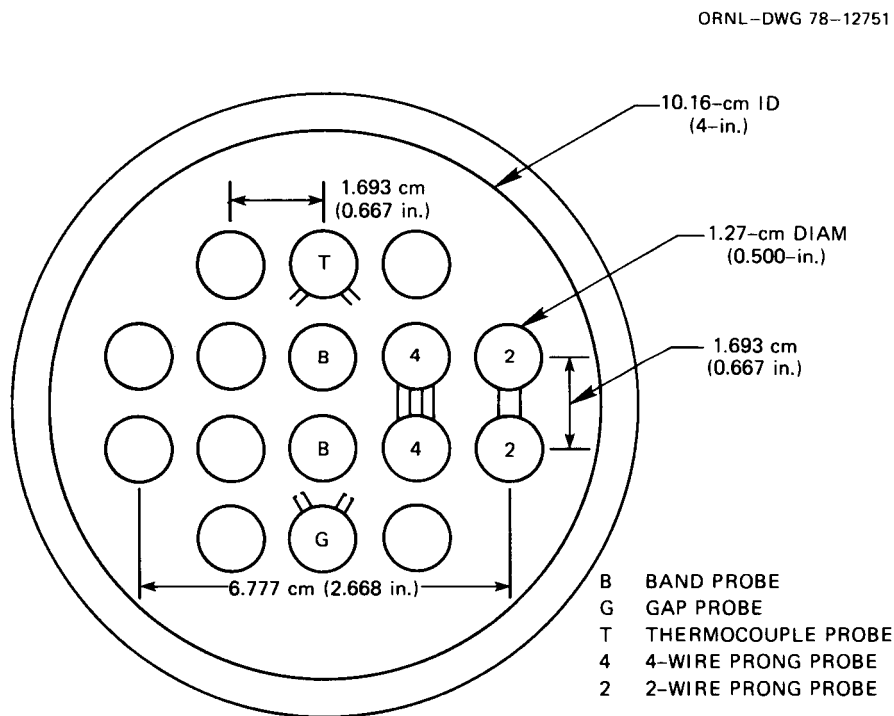


Fig. 25. Details of various instrumented rods tested in Bundle 1 (arrangement of probes).

geometrical scale-up of a PWR bundle consisting of 10.72-mm (0.422-in.) diameter tubes in a rectangular array with a center-to-center distance between rods of 14.3 mm (0.563 in.). The bundle was installed in the air-water two-phase loop and run in the vertical upflow mode. The loop instrumentation for the in-bundle probe test series was the same as that in Table 2, except that the drag disk was omitted.

Three steady-state runs of approximately 20 min each were made for void fraction measurements. The air and water flow rates and void fractions as measured by the gamma densitometer and Auburn meter are shown in Table 8.

Table 8. Air and water flow rates and their resultant void fraction for Bundle 1 testing

Test No.	Air flow		Water flow		Void fraction	
	[m ³ /sec	(scfm)]	[m ³ /sec	(gpm)]	D	Auburn
1	0.00283	(6)	0.0126	(200)	0.164	0.360
2	0.0151	(32)	0.0063	(100)	0.583	0.862
3	0.1208	(256)	0.0032	(50)	0.881	0.975

7.2 Bundle 1 Data Reduction and Analysis

In analyzing the results, the void fraction determined by gamma densitometer data was used to calculate the liquid and vapor velocities in the 16-rod bundle. The results of the noise analysis and liquid and vapor velocities from the measured single phase flows and gamma densitometer values for the various impedance probes are shown in Table 9.

Before proceeding with a detailed discussion of these results, it would be worthwhile to take a closer look at Fig. 25, which shows the

Table 9. Liquid and vapor velocities from metered in-flow and the gamma densitometer compared with noise-analysis velocity for various in-bundle impedance probes

Run No.	Void fraction density	Velocities from gamma densitometer and metered in-flow rates		Band probe width (in.)			4-wire probe spacing (in.)			2-wire probe level	Gap probe level
		V_g (fps)	V_f (fps)	1/16	3/16	3/8	2	1	1/2	3 & 4	1 & 2
1	0.161	9.65	5.75	7.7	7.7	7.6	4.5	3.7	5.2	7.2	8.1
2	0.583	9.41	5.79	8.38	-	8.44	10.9	4.6	5.1	7.9	8.1
3	0.881	50.03	10.19	-	15.0	-	11.2	6.3	7.3	9.8	15.5

arrangement of in-bundle probes in the 16-rod bundle. As shown, the bundle is far enough from the inside edge of the 10.16-cm-ID (4 in.) plastic pipe surrounding the bundle for a measurable variation to exist between the flow in the inside subchannels (between the rods) and the exterior subchannel (between the rod bundle and the pipe). The velocity difference between the exterior and interior channels can be written as

$$\frac{V_{\text{exterior}}}{V_{\text{interior}}} = \left(\frac{D_{H \text{ exterior}}}{D_{H \text{ interior}}} \right)^{2/3}$$

for turbulent, fully developed flow. The velocities listed in Table 9 are those of the interior subchannels where the probes were located.

8. AIR-WATER TESTING SUMMARY AND CONCLUSIONS

J. E. Hardy* P. A. Jallouk*
M. B. Herskovitz W. H. Leavell

From the two-phase flow studies made to date, the liquid and vapor velocities determined from the inlet air and water flow rates and gamma densitometer agree with those of several of the slip models in the literature (especially that of Govier and Aziz⁷). The string probe yielded a noise-analysis velocity which lay in between that of the liquid and vapor in the void fraction range up to 0.80. The application of a simple method developed to extract the liquid velocity from the noise-analysis value yields encouraging results. The use of the adaptive cross-correlation algorithm in tracking both the 1-min and the 30-sec transients yielded noise analysis values that also lay between the liquid and vapor velocities.

The use of a conductivity measurement to determine void fraction yielded good agreement with a gamma densitometer. This technique, however, is not very reliable, since it is based on a knowledge of water conductivity, which is very temperature dependent.

The same trends noted for the string probe two-phase flow velocities are also applicable to the in-bundle results.

* Engineering Technology Division.

9. ELECTRONIC CIRCUIT DEVELOPMENT

M. J. Roberts
W. H. Andrews R. G. Phillips
W. E. Lingar E. W. Walker, Jr
W. R. Miller

Several conceptual designs of impedance and film probes were fabricated (as reported in the sections on development of film probes, string probes, and in-bundle probes), and their electrical characteristics were tested in water and air. The test results, along with a theoretical study of water properties, point to an electrical model for these probes in the form of a resistance and a capacitance connected in parallel. The resistance and the capacitance are both functions of the conductivity and permittivity of the medium between the two elements of the sensor. The conductivity and permittivity vary as the void fraction of the two-phase fluid varies. Unfortunately, the conductivity and permittivity are also functions of the ion concentration and the temperature of the water, which must also be measured unless their effects can be shown to be negligible on either conductivity or permittivity during a test. Since the exact effects of ion concentration and temperature on conductivity and permittivity were not well known, the decision was made to develop the electronics with the capability to measure both resistance and capacitance in order to acquire the maximum amount of information.

Three promising electronic techniques were considered. One, used in a commercial product, has the sensor as part of the tuned circuit in an oscillator. As the sensor capacitance changes, the oscillator frequency changes; so an FM demodulator yields a voltage proportional to capacitance. This concept measures only capacitance and will work only

if the resistance is quite large (as in high-purity water); another problem occurs if the cable capacitance changes (due perhaps to temperature variations). That change will be interpreted as a change in sensor capacitance. The effect of the cable could be rejected if another identical cable without a sensor is placed near the sensor cable, and the capacitance variation with temperature between cables is tracked very precisely. By connecting each cable to an identical oscillator and mixing the oscillator outputs, a difference frequency that would be independent of the cable capacitances is obtained. However, in limited tests of a ceramic-insulated cable, it was found that the cable capacitance variation with temperature does not track well between two cables. For this reason, and because only one component, capacitance, is measured in the best of circumstances, this concept was rejected.

The second concept was to design a self-balancing impedance bridge. By this technique, one can make a three-terminal measurement that inherently eliminates the effect of cable capacitance (but only when the bridge is at null) and measures both resistance and capacitance. Commercial instruments that self-balance are available, but their speed of response is very limited (less than 20 samples per second). In concept, at least, a fast self-balancing bridge could be developed. In this concept, a varactor diode and a field-effect transistor (FET) provide the adjustable capacitance and resistance, respectively. Voltage is sensed, separated into in-phase and quadrature components, and fed back to the diode and FET transistor to maintain null as resistance and capacitance vary. At null the cable capacitance has no effect because one portion has no voltage across it and the other is being driven from a very low impedance

source. One problem with this concept is that relations between the feedback voltages and the capacitance of the diode and the resistance of FET transistor are nonlinear and vary from device to device. Also, since the concept is very new and untried at ORNL and would therefore require a long development effort, it has been put aside, at least temporarily.

The third concept, the one chosen for development, is the use of a "driven shield" to eliminate cable capacitance problems. This concept is illustrated schematically in Fig. 26. The probe is excited at 100 kHz through a triaxial cable. The inner shield of the triax cable is driven at the same potential as the center conductor so that the cable capacitance does not appear in the gain expression for the first stage of the preamplifier. A second stage increases the sensitivity of the measurement by amplifying the difference between the driving voltage and the output of the first stage. The second-stage output is synchronously demodulated with reference to the oscillator voltage, both in-phase and quadrature, to produce outputs proportional to the sensor resistance and capacitance. The output filters remove the 100 kHz carrier from these signals.

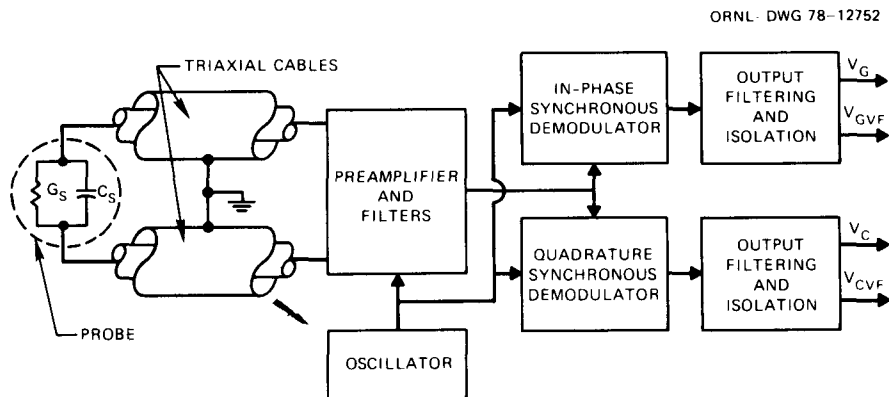


Fig. 26. Electronic system developed for probe impedance measurement.

10. ADVANCED INSTRUMENTATION FOR REFLOOD STUDIES
STEAM-WATER TEST STAND

J. A. Conlin* P. P. Haydon* H. R. Payne[†]

The Steam-Water Test Stand is necessary to duplicate as closely as possible the two-phase flow condition within the reflow facilities. This is to be used as one of the final tests to ensure the quality and integrity of the finished instrument systems before shipment.

The design for various subsystems of the (AIRS) Steam-Water Test Stand is under way; the parameters for this facility are presented in Table 10. The impedance probe assemblies will be checked in a two-phase steam-water flow. The design was completed and construction is under way on the facility's demineralized water and steam supply lines. The Steam-Water Test Stand configuration is shown in Fig. 27. Design of the loop piping is nearly complete, and the test section design is under way. Obtaining spacer grids (for the testing of instrumented rods) on the timely basis required to complete the Test Stand has been a problem. Procurement of most other long-lead materials for the Test Stand has been initiated, however.

* Engineering Technology Division.

† UCC-ND Engineering Division.

Table 10. AIRS Steam-Water Test Stand design parameters

<u>Steam-Water Data</u>	
Design pressure	1034 kPa (150 psig)
Design temperature	185°C (365°F)
Operating pressure range	0-689 kPa (0-100 psig)
Operating temperature range	Ambient-170°C (338°F)
Steam flow	4032 kg/hr (9000 lb/hr)
Steam velocity	3048 m/s (100 fps)
Mixed flow void fraction	0-100%
Water flow	0-45.60 liters/min (0-12 gpm)
<u>Mechanical Data</u>	
Overall height	~9.141 m (~30 ft)
Test section length	5.791 m (19 ft)
Test section diameter	89.90 mm (3.54 in.)
<u>Facility Parameters</u>	
Water temperature, pressure, and flow	
Steam temperature, pressure, and flow	
Lighted viewports at two elevations	
Water conductivity	
Special instrumented spool piece for data in the mixed- flow region.	} Three-beam gamma densitometer (density) } Turbine flowmeter (velocity) } Drag disks (momentum flux)

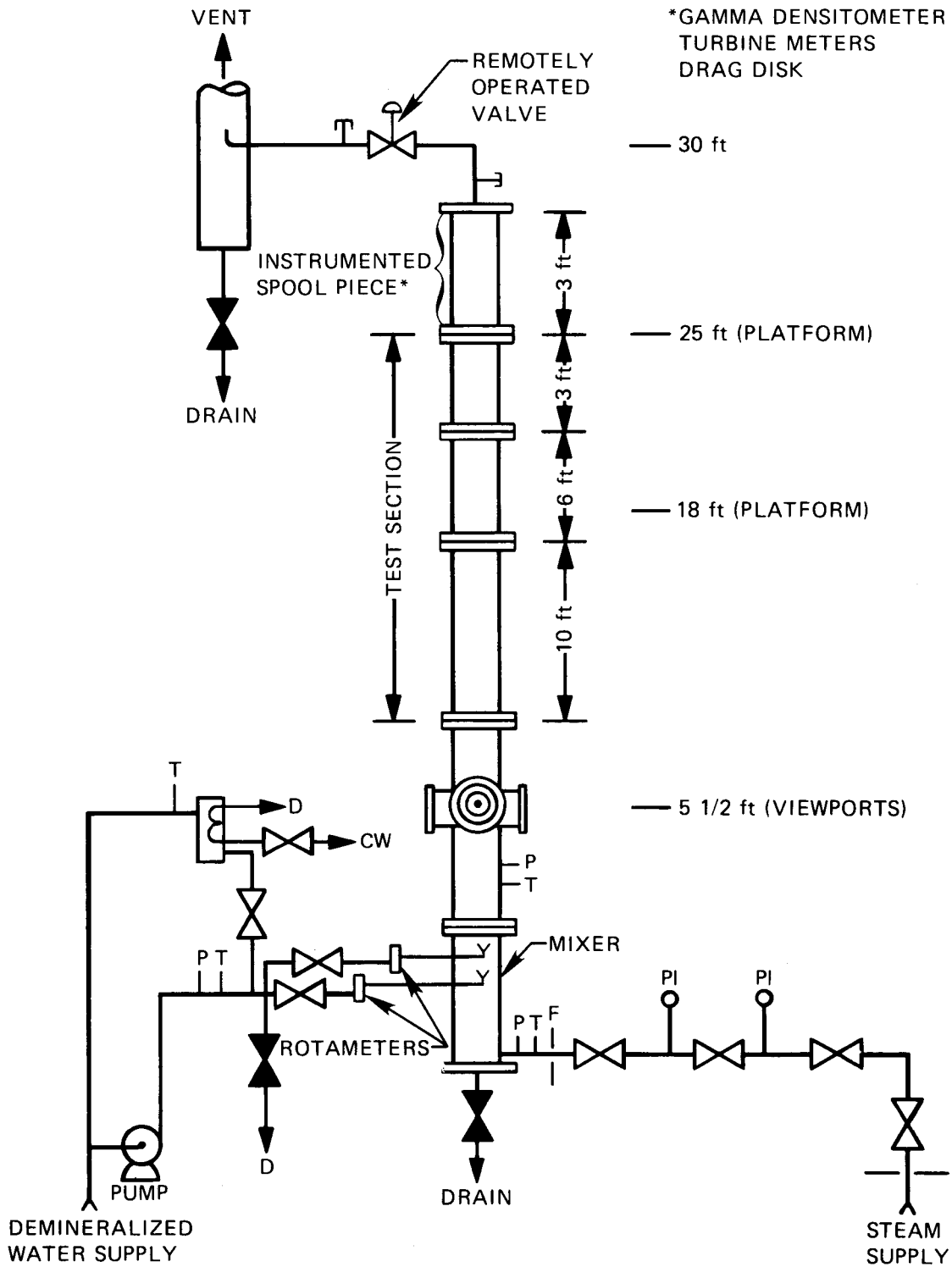


Fig. 27. AIRS Steam-Water Test Stand.

REFERENCES

1. G. Carrard and T. J. Ledwidge, "Measurement of Slip Distribution and Average Void Fraction in an Air-Water Mixture," Proceedings of the International Symposium on Two-Phase Systems, Vol. 6, Progress in Heat and Mass Transfer, Haifa, 1971, Pergamon Press (1972).
2. J. D. Sheppard et al., Quarterly Progress Report on Advanced Two-Phase Instrumentation Program for November-December 1976, ORNL/NUREG/TM-93.
3. W. H. Leavell et al., Advanced Two-Phase Instrumentation Program Quarterly Progress Report for April-June 1977, ORNL/NUREG/TM-140.
4. P. A. Jallouk et al., Advanced Two-Phase Instrumentation Program Quarterly Progress Report for July-September 1977, ORNL/NUREG/TM-183.
5. M. Merit et al., "Void Fraction Measurement with a Rotating Electric Field Conductance Gauge," Trans. ASME 99, 330-32 (May 1977).
6. D. G. Thomas et al., Quarterly Progress Report on Blowdown Heat Transfer Separate-Effects Program for January-March 1977, ORNL/NUREG/TM-120.
7. G. W. Govier and K. Aziz, The Flow of Complex Mixtures in Pipes, Van Nostrand Reinhold Company, New York, 1972.
8. G. A. Hughmark and B. S. Pressburg, "Holdup and Pressure Drop with Gas-Liquid Flow in a Vertical Pipe," AIChE J. 7(4), 677-81 (1961).
9. G. A. Hughmark, "Holdup in Gas-Liquid Flow," Chem. Eng. Prog. 58(4), 62-65 (April 1962).
10. R. C. Martinelli and D. B. Nelson, "Prediction of Pressure Drop during Forced-Circulation of Boiling Water," Trans. ASME 70(6), 695-702 (August 1944).
11. J. R. S. Thom, "Prediction of Pressure Drop during Forced Circulation Boiling of Water," Int. J. Heat Mass Transfer 7(7), 709-24 (July 1964).
12. S. G. Bankoff, "A Variable Density Single-Fluid Model for Two-Phase Flow with Particular Reference to Steam-Water Flow," Trans. ASME, J. Heat Transfer 82(4), 265-72 (November 1960).
13. G. A. Hughmark, "Holdup in Gas-Liquid Flow," Chem. Eng. Prog. 58(4), 62-65 (April 1962).
14. D. G. Thomas et al., Quarterly Progress Report on Blowdown Heat Transfer Separate-Effects Program for January-March 1976, ORNL/NUREG/TM-14.

15. D. G. Thomas et al., Quarterly Progress Report on Blowdown Heat Transfer Separate-Effects Program for October-December 1977, ORNL/NUREG/TM-134.

NUREG/CR-0213
ORNL/NUREG/TM-202
Dist. Category R2

Internal Distribution

- | | | | |
|------|------------------|--------|-------------------------------|
| 1. | W. H. Andrews | 22. | C. S. Morgan |
| 2. | R. S. Booth | 23. | C. A. Mossman |
| 3. | M. E. Buchanan | 24. | F. R. Mynatt |
| 4. | J. A. Conlin | 25. | F. H. Neill |
| 5. | W. B. Cottrell | 26. | H. R. Payne |
| 6. | I. T. Dudley | 27. | C. J. Remenyik |
| 7-8. | B. G. Eads | 28. | M. J. Roberts |
| 9. | R. P. Gates | 29. | M. R. Sheldon |
| 10. | G. W. Greene | 30. | R. L. Shipp |
| 11. | J. E. Hardy | 31. | A. N. Smith |
| 12. | M. B. Herskovitz | 32. | J. W. Spitzer |
| 13. | H. N. Hill | 33. | J. D. Stout |
| 14. | J. H. Holladay | 34. | L. H. Thacker |
| 15. | J. L. Horton | 35. | D. G. Thomas |
| 16. | J. O. Hylton | 36. | H. E. Trammell |
| 17. | P. A. Jallouk | 37. | ORNL Patent Office |
| 18. | W. H. Leavell | 38-39. | Central Research Library |
| 19. | W. E. Lingar | 40. | Document Reference Section |
| 20. | W. R. Miller | 41-45. | Laboratory Records Department |
| 21. | A. J. Moorhead | 46. | Laboratory Records (RC) |

External Distribution

47. Y. Y. Hsu, Systems Engineering Branch, Division of Reactor Safety Research, Nuclear Regulatory Commission, Washington, D.C. 20555
48. Director, Reactor Division, DOE, ORO
49. Director, Research and Technical Support Division, DOE, ORO
- 50-409. Given distribution as shown under category R2 (25 copies - NTIS)